TITLE: Organelle proteomic profiling reveals lysosomal heterogeneity in association with longevity

AUTHOR: Yong Yu[1,2,#,*], Shihong M. Gao[3,4,#], Youchen Guan[4,5,#], Pei-Wen Hu[2], Qinghao Zhang[2], Jiaming Liu[1], Bentian Jing[1], Qian Zhao[2], David M Sabatini, Monther Abu-Remaileh[6], Sung Yun Jung[7], Meng C. Wang[2,4,*]

1. Current address: State Key Laboratory of Cellular Stress Biology, School of Life Sciences, Faculty of Medicine and Life Sciences, Xiamen University, Xiamen 361102, China

2. Huffington Center on Aging, Baylor College of Medicine, Houston TX, USA 77030

3. Developmental Biology Graduate Program, Baylor College of Medicine, Houston TX, USA 77030

4. Janelia Research Campus, Howard Hughes Medical Institute, Ashburn VA, USA 20147

5. Molecular and Cellular Biology Graduate Program, Baylor College of Medicine, Houston TX, USA 77030

6. Department of Chemical Engineering, Stanford University, Stanford CA, USA 94305

7. Department of Molecular and Cellular Biology, Baylor College of Medicine, Houston TX, USA 77030

# Equal contribution

* Correspondence and requests for materials should be addressed to Meng C. Wang (mengwang@janelia.hhmi.org) or Yong Yu (yuy@xmu.edu.cn)

ABSTRACT

Lysosomes are active sites to integrate cellular metabolism and signal transduction. A collection of proteins enriched at lysosomes mediate these metabolic and signaling functions. Both lysosomal metabolism and lysosomal signaling have been linked with longevity regulation; however, how lysosomes adjust their protein composition to accommodate this regulation remains unclear. Using large-scale proteomic profiling, we systemically profiled lysosome-enriched proteomes in association with different longevity mechanisms. We further discovered the lysosomal recruitment of AMPK and nucleoporin proteins and their requirements for longevity in response to increased lysosomal lipolysis. Through comparative proteomic analyses of lysosomes from different tissues and labeled with different markers, we discovered lysosomal heterogeneity across tissues as well as the specific enrichment of the Ragulator complex on Cystinosin positive lysosomes. Together, this work uncovers lysosomal proteome heterogeneity at different levels and provides resources for understanding the contribution of lysosomal proteome dynamics in modulating signal transduction, organelle crosstalk and organism longevity.

INTRODUCTION

Lysosomes are membrane-bound organelles that are specialized to constitute an acidic environment in the cytosol. Lysosomes carry a large number of proteins that are essential for maintaining lysosomal activities and mediating lysosomal regulatory effects. Inside the lysosomal lumen, a series of acidic hydrolases, including lipases, proteases, glucosidase, acid phosphatase, nuclease and sulfatases, are responsible for the degradation and recycling of extracellular and intracellular materials delivered through endocytic, phagocytotic and

47 autophagic processes (Appelqvist et al., 2013; Ballabio & Bonifacino, 2020; Lawrence & Zoncu,
48 2019). On the membrane that encloses the lysosome, a group of integral transmembrane proteins
49 play crucial roles in the maintenance of luminal acidic pH and ion homeostasis, in the control of
50 lysosomal membrane potential and export of metabolic products, as well as in the regulation of
51 organelle interaction and signal transduction (Ballabio & Bonifacino, 2020; Lawrence & Zoncu,
52 2019). For example, lysosomal vacuolar-type H^+-ATPase (v-ATPase) on the membrane is the
53 primary driver for the active accumulation of protons in the lysosomal lumen, which also
54 requires a neutralizing ion movement mediated by ion channels and transporters (Graves et al.,
55 2008; Nicoli et al., 2019). In addition, v-ATPase coordinates with lysosomal amino acid
56 transporter SLC38A9 and lysosomal cholesterol exporter NPC1 in regulating the activation of
57 mechanistic/mammalian target of rapamycin complex I (mTORC1) by amino acid and lipid cues
58 (Castellano et al., 2017; Wang et al., 2015). The recruitment of mTORC1 to the lysosome is
59 mediated by RagA/B and RagC/D GTPase heterodimers that are associated with the scaffold
60 protein complex Ragulator tethered on the lysosomal membrane (de Araujo et al., 2017).
61 Through interacting with Axin, Ragulator also mediates the activation of AMP-activated protein
62 kinase (AMPK) on the lysosomal surface (Zhang et al., 2014). Furthermore, lysosomes are not
63 static, isolated organelles; instead they are highly mobile vesicles that undergo frequent
64 movements in both anterograde (nucleus-to-periphery) and retrograde (periphery-to-nucleus)
65 directions and form dynamic interactions with other organelles including endosomes,
66 autophagosomes, endoplasmic reticulum and mitochondria (Ballabio & Bonifacino, 2020; Pu et
67 al., 2016). These trafficking and interaction processes are mediated by lysosomal integral
68 transmembrane proteins as well as diverse proteins that are recruited to lysosomes in response to
69 different extracellular and intracellular inputs (Ballabio & Bonifacino, 2020; Pu et al., 2016).

70

71 Lysosomes control numerous cellular processes, and dysfunction of lysosomes has been linked
72 with various diseases, such as lysosomal storage disorders (Ballabio & Gieselmann, 2009; Platt
73 et al., 2012), Alzheimer's disease (Nixon & Cataldo, 2006) and some types of cancer (Davidson
74 & Vander Heiden, 2017; Fehrenbacher & Jaattela, 2005). Emerging evidences also reveal the
75 lysosome as a central regulator of organism longevity, through its involvement in autophagy and
76 its modulation of metabolic signaling pathways. The induction of autophagic flux has been
77 observed in multiple pro-longevity circumstances, and is required for the pro-longevity effects
78 caused by those genetic, dietary and pharmacological interventions, such as reduced insulin/IGF-
79 1 signaling, caloric restriction and spermidine treatment (Hansen et al., 2018). On the other hand,
80 lysosomes are now recognized as the key platform to modulate the activities of mTORC1 and
81 AMPK signaling, two well-characterized longevity regulatory pathways (Savini et al., 2019). In
82 addition, our studies have discovered lysosomal lipid messenger pathways that are induced by a
83 lysosomal acid lipase LIPL-4 and promote longevity via both cell-autonomous and cell-
84 nonautonomous signaling mechanisms (Folick et al., 2015; Ramachandran et al., 2019; Savini et
85 al., 2022; Wang et al., 2008). Given the importance of lysosomes in regulating longevity, it will
86 be crucial to understand how changes in the lysosomal protein composition are associated with
87 longevity regulation.

88

89 To systemically profile the protein composition of lysosomes, methods have been developed to
90 purify lysosomes using gradient centrifugation (Gao et al., 2017; Lubke et al., 2009; Markmann
91 et al., 2017; Schroder et al., 2010). More recently, a lysosome immunoprecipitation method,
92 which uses anti-HA (human influenza virus hemagglutinin) antibody conjugated magnetic beads

93 to immune-purify lysosomes from mammalian cells expressing transmembrane protein 192
94 (TMEM192) fused with three tandem HA (3×HA) epitopes, has further improved the specificity
95 and speed of lysosomal isolation (Abu-Remaileh et al., 2017). This rapid isolation method has
96 greatly facilitated follow-up mass-spectrometry (MS) based proteomics as well as metabolomics
97 analyses (Abu-Remaileh et al., 2017; Eapen et al., 2021; Laqtom et al., 2022).
98
99 In the present study, we have applied an immunoprecipitation-based method for rapid isolation
100 of lysosomes from live *C. elegans* using transgenic strains expressing lysosomal membrane
101 proteins tagged with 3×HA (Lyso-Tag). We then conducted large-scale proteomic profiling using
102 isolated lysosomes and remaining non-lysosomal fractions, to determine the enrichment of each
103 identified protein on the lysosome. Based on these analyses, we have defined a lysosome-
104 enriched proteome and compared it between wild-type and long-lived worms, revealing
105 lysosomal protein composition changes associated with longevity. We have also generated
106 transgenic strains expressing Lyso-Tag specifically in the hypodermis (epidermal), muscle,
107 intestine (fat storage/digestion) and neurons, leading to the discovery of lysosomal proteome
108 heterogeneity in different tissues. Furthermore, by comparing the lysosome-enriched proteome
109 with LAMP1/LMP-1 Lyso-Tag and the one with Cystinosin/CTNS-1 Lyso-Tag, we discovered
110 that the Ragulator complex and other mTORC1 regulators exhibit increased enrichments on
111 lysosomes containing the cysteine transporter Cystinosin.
112
113 **RESULTS**
114
115 **Map lysosome-enriched proteome systemically in *C. elegans***

116

117 In order to comprehensively reveal proteins that are enriched at the lysosome, we have applied
118 rapid lysosome immunoprecipitation followed by MS-based proteomic profiling (Lyso-IP)
119 (Figure 1A). We first generated a transgenic strain expressing the lysosome-associated
120 membrane protein, LMP-1 (Eskelinen, 2006) tagged with both 3×HA and RFP (LMP-1 *LysoTg*).
121 Fluorescence imaging of RFP confirmed the lysosomal localization of the LMP-1 fusion protein
122 in live organisms and made it possible to follow purified lysosomes *in vitro* (Figure 1B). The
123 3×HA epitope tag is used to purify lysosomes from homogenized worm lysate via
124 immunoprecipitation using anti-HA antibody conjugated magnetic beads (Figure 1A). In general,
125 about 160,000 worms at day-1 adulthood were harvested and homogenized. Upon centrifuge to
126 remove debris and nuclei, 3×HA-tagged lysosomes were immunoprecipitated and separated from
127 other cellular content (flow-through controls, Figure 1A). The whole process from harvested
128 worms to purified lysosomes takes around 25 minutes. Many purified lysosomes were able to
129 take up LysoTracker probes and exhibit positive fluorescence signals, indicating that they
130 maintain intact with an acidic pH; while there are also some broken lysosomes losing
131 LysoTracker staining (Figure 1C). When blotting with antibodies against different organelle
132 markers, we found that the purified lysosomes show no or nearly no protein markers of other
133 organelles, including HSP-60 (mitochondria heat shock protein) (Hartl et al., 1992; Mayer,
134 2010), CYP-33E1 (Endoplasmic Reticulum (ER) cytochrome P450) (Brown & Black, 1989),
135 SQV-8 (Golgi glucuronosyltransferase) (Hadwiger et al., 2010) and beta-actin (cytoskeleton)
136 (Figure 1D), while the flow-through controls show these protein markers but nearly no lysosomal
137 protein marker LMP-1 (Figure 1D). Together, these results demonstrate the efficacy of the Lyso-
138 IP approach to enrich lysosome proteins.

139

140 Next, we conducted proteomic profiling of purified lysosomes with their paired flow-through
141 controls (Figure 1A). The correlation analysis shows good repeatability among four independent
142 biological replicates (Supplementary Figure 1A), and the PCA analysis shows a clear separation
143 between Lyso-IP replicates and flow-through controls (Figure 1E). In parallel, we also conducted
144 immunoprecipitation using homogenized lysate from wild-type (WT) worms that do not carry a
145 Lyso-Tag and then analyzed proteomic profiles of three independent samples as non-tag controls
146 (Figure 1A). Based on these proteomic data, we used three criteria to identify lysosome-enriched
147 proteins: first, their levels in the purified lysosomes are 10-fold or higher than those in the flow-
148 through controls (Figure 2A); second, their enrichments can be repeated in all biological
149 replicates (Figure 2A); and lastly, their enrichments over non-tag controls are more than 2-fold
150 (Figure 2B).

151

152 Together, 216 lysosome-enriched candidates were identified from more than 6000 detected
153 proteins, and 178 candidates have mammalian homologs (Supplementary Figure 1B,
154 Supplementary Table 1). This lysosome-enriched proteome consists of 83 membrane transporters
155 and channels, 47 enzymes, 26 signaling factors, 12 structural components, and 6 involved in
156 vesicle trafficking (Figure 2C). These include known lysosomal proteins, such as various
157 lysosomal Cathepsins that catalyze protein degradation (Turk et al., 2012), lysosomal specific
158 ARL8 GTPase that mediates lysosome trafficking (Nakae et al., 2010), and subunits of
159 lysosomal v-ATPase that pumps protons into the lysosomal lumen to maintain an acidic pH
160 (Forgac, 2007) (Supplementary Table 1).

161

162 Lysosomal v-ATPase consists of both V0 and V1 domains that are associated with the lysosomal
163 membrane and faced the cytosol, respectively. Reversible dissociation of the V1 and V0 domains
164 responds to nutritional signals and plays a crucial role in the regulation of the lysosomal v-
165 ATPase activity (Kane, 1995; McGuire & Forgac, 2018; Ratto et al., 2022; Stransky & Forgac,
166 2015). Except for VHA-18 (V1 H subunit), we were able to detect all other subunits of
167 lysosomal v-ATPase, including VHA-5, 6, 7 and UNC-32 (V0 a subunits), VHA-1, 2, 3 and 4
168 (V0 c subunits), VHA-16 (V0 d subunit), VHA-17 (V0 e subunit), VHA-13 (V1 A subunit),
169 VHA-12 (V1 B subunit), VHA-11 (V1 C subunit), VHA-14 (V1 D subunit), VHA-8 (V1 E
170 subunit), VHA-9 (V1 F subunit), VHA-10 (V1 G subunit), and VHA-15 (V1 H subunit), and
171 also two v-ATPase transporting accessory proteins, VHA-19 and VHA-20 (Figure 2D,
172 Supplementary Table 1). Among the V0 domain subunits, VHA-4, 5, 6, 7 and 16 and UNC-32
173 are enriched over 10-fold in all four replicates, VHA-1, 2 and 3 are enriched over 10-fold in
174 three replicates and over 5-fold in one replicate, and the low abundant VHA-17 was only
175 detected in two replicates, with more than 10-fold enrichments in both (Figure 2D). The VHA-19
176 transporting accessory protein is enriched over 10-fold in two replicates and less than 5-fold in
177 two replicates (Figure 2D). In contrast, for the subunits of the V1 domain and the VHA-20
178 transporting accessory protein, they show no enrichment in the purified lysosomes compared to
179 the flow-through controls (Figure 2D). These results suggest that the free form of the V1 domain
180 and the associated form bound with the V0 domain at lysosomes both exist under the well-fed
181 condition in wild-type worms.
182
183 In addition to 30.7% of proteins with known lysosome/endosome localization, the lysosome-
184 enriched proteome includes a small portion of proteins localized to other cellular organelles,

185 ER/Golgi (6.0%), mitochondria (1.4%), peroxisome (0.4%), lipid droplet (0.9%), and synaptic
186 vesicle (1.8%) (Figure 2E). On the other hand, there is a large portion of proteins with annotated
187 plasma membrane localization (24.8%) (Figure 2E). Many of these plasma membrane proteins
188 are receptors that are known to be subject to endocytosis and subsequent recycling lysosomal
189 degradation, such as INA-1/integrin alpha-6 (De Franceschi et al., 2015), VER-3/vascular
190 endothelial growth factor receptor (Ewan et al., 2006), PTC-1/protein patched receptor (Gallet &
191 Therond, 2005), and IGLR-2/leucine-rich repeat-containing G-protein coupled receptor (Snyder
192 et al., 2013) (Supplementary Table 1) (Braulke & Bonifacino, 2009). We also identified proteins
193 involved in the endocytosis process, including low-density lipoprotein receptor-related proteins,
194 LRP-1 (Grant & Hirsh, 1999) and arrestin domain-containing proteins, ARRD-13 and ARRD-18
195 (Kang et al., 2014) (Supplementary Table 1) that mediate the internalization of plasma
196 membrane receptors (Ma et al., 2002). Thus, the lysosome-enriched proteome also reveals
197 membrane receptor proteins that undergo recycling through the endo-lysosomal system.
198
199 **Lysosome-enriched proteome alterations associate with longevity**
200

201 Lysosomes are known as a heterogeneous population of vesicles, differing in their size, shape,
202 pH and cellular distribution. Considering the emerging role of lysosomes as a cellular hub to
203 integrate protein signals and regulate longevity, we expect that the protein composition of
204 lysosomes may exhibit heterogeneity in association with different longevity mechanisms. To test
205 this hypothesis, we crossed LMP-1 *LysoTg* with the long-lived *lipl-4* transgenic strain (*lipl-4 Tg*)
206 that constitutively expresses a lysosomal acid lipase (Wang et al., 2008) and also the long-lived
207 loss-of-function mutant of *daf-2* (*daf-2(lf)*) that encodes the insulin/IGF-1 receptor (Kenyon et

208 al., 1993; Martins et al., 2016). Reducing insulin/IGF-1 signaling is a well-conserved mechanism
209 to promote longevity in diverse organisms ranging from *C. elegans, Drosophila,* mice to humans
210 (Kenyon et al., 1993; Martins et al., 2016). We conducted Lyso-IP proteomic analyses and
211 compared lysosome-enriched proteomes between wild-type and long-lived strains. The
212 correlation analysis shows good repeatability among three independent biological replicates
213 (Supplementary Figure 1C, 1D), and the PCA analysis shows a clear separation between Lyso-IP
214 replicates and flow-through controls (Supplementary Figure 1E).
215
216 Using LMP-1 Lyso-IP, we have identified 449 lysosome-enriched proteins in the *lipl-4 Tg*
217 worms (Supplementary Table 2), and 176 of them overlap with the LMP-1 Lyso-IP candidates
218 from WT worms (Figure 3A). Thus, 82% of proteins enriched at WT lysosomes are also
219 enriched at *lipl-4 Tg* lysosomes; however, 61% of proteins enriched at *lipl-4 Tg* lysosomes are
220 absent at WT lysosomes (Figure 3A). Interestingly, among the proteins that are specific to *lipl-4*
221 *Tg* lysosomes, there are autophagosome proteins and proteins that mediate the fusion between
222 autophagosomes and lysosomes, including ATG-9/ATG9A(Popovic & Dikic, 2014), EPG-
223 7/RB1CC1 (Nishimura et al., 2013), VAMP-7/VAMP8 (Diao et al., 2015; Itakura et al., 2012)
224 and Y75B8A.24/PI4KIIα (Sugiura et al., 1989) (Figure 3B), suggesting that autophagy is
225 induced by *lipl-4 Tg*. Consistently, the induction of autophagy has been reported in the *lipl-4 Tg*
226 worms, which is required for the longevity effect (Lapierre et al., 2011).
227
228 In addition, we found that the Ragulator complex, LMTR-2/LAMTOR2, LMTR-3/LAMTOR3
229 and LMTR-5/LAMTOR5, that serves as a scaffold for the activation of mTORC1 and AMPK
230 (Zhang et al., 2014) is more specifically enriched at the lysosome from the *lipl-4 Tg* worms than

231 WT (Figure 3B). There are two homologs of AMPK catalytic units, AAK-1 and AAK-2 in *C.*
232 *elegans.* We found that AAK-2 is enriched more than 10-fold in the Lyso-IP samples compared
233 to the flow-through controls from the *lipl-4 Tg* worms, but it is only detected in the flow-through
234 controls from WT worms (Figure 3C). Likely due to its low abundance, AAK-1 was detected
235 twice in the Lyso-IP samples from the *lipl-4 Tg* worms but once only in the flow-through sample
236 from WT worms (Figure 3C). These results suggest that AMPK is specifically recruited to the
237 lysosomal surface and becomes activated to promote longevity in the *lipl-4 Tg* worms. In
238 supporting this idea, we found that the inactivation of AMPK using the *aak-2* loss-of-function
239 mutant together with the *aak-1* RNA interference (RNAi) knockdown reduces the lifespan
240 extension in the *lipl-4 Tg* worms from 72% to 40% (Figure 3D, Supplementary Table 3). Thus,
241 the lysosomal activation of AMPK responds to LIPL-4-induced lysosomal lipolysis and mediates
242 the longevity regulation.
243
244 Moreover, compared to WT lysosomes, the enrichment of lysosomal v-ATPase is higher in *lipl-4*
245 *Tg* lysosomes, especially for the V0 subunits, VHA-1, 2, 3 the V1 subunits, VHA-11 and VHA-
246 15, and the v-ATPase transporting accessory proteins, VHA-19 and VHA-20 (Figure 3B). There
247 are also 13 lysosomal channels/transporters, including T14B4.3/ATP6AP2, the proton-
248 translocating ATPases required for the v-ATPase-mediated lysosomal acidification (Cruciat et
249 al., 2010) and CLH-6/CLCN7, the H(+)/Cl(-) exchange transporter mediating the acidification of
250 the lysosome (Graves et al., 2008; Nicoli et al., 2019), and 16 lysosomal hydrolases that are
251 specifically associated with the *lipl-4 Tg* lysosomes (Figure 3B). Together, these results suggest
252 that the proportion of mature lysosomes is increased in the *lipl-4 Tg* worms, which may lead to

253 increased autophagy, the lysosomal activation of AMPK, and consequently the induction of
254 longevity.
255
256 In parallel, 259 lysosome-enriched proteins were identified in the *daf-2(lf)* mutant using LMP-1
257 Lyso-IP (Supplementary Table 4), 147 of them overlapping with the LMP-1 Lyso-IP candidates
258 from WT worms, 197 of them overlapping with the LMP-1 Lyso-IP candidates from the *lipl-4*
259 *Tg* worms, and 55 unique to the *daf-2(lf)* mutant (Figure 3A). The *daf-2(lf)* lysosome-enriched
260 proteome shows enrichment of autophagic components, including ATG-9/ATG9A (also shown
261 in *lipl-4 Tg* lysosome-enriched proteome) and the autophagy receptor SQST-1/SQSTM1 (Figure
262 3B), which supports the previously reported induction of autophagy in the *daf-2(lf)* mutant. On
263 the other hand, the Ragulator complex components LMTR-2/3/5 were not more enriched in the
264 lysosome from the *daf-2(lf)* mutant than that from WT worms (Figure 3B). For the AMPK
265 catalytic subunits, AAK-2 was not identified in the lysosome-enriched proteome from the *daf-*
266 *2(lf)* mutant, and the low abundant AAK-1 was not detected in either Lyso-IP or flow-through
267 samples (Figure 3C). It is known that the activation of AMPK displays high spatial specificity in
268 the cell when responding to different upstream stimuli (Khan & Frigo, 2017). In *C. elegans,* it
269 was previously shown that AAK-2 mediates the longevity effect conferred by the *daf-2(lf)*
270 mutant (Apfeld et al., 2004). Our results indicate that this regulation might not be associated with
271 the lysosomal activation of AMPK. Thus, the spatial specificity of AMPK activation at different
272 subcellular compartments may be linked with different longevity mechanisms.
273
274 **Enhanced lysosome-nucleus interaction mediates longevity**
275

276 In our previous studies, we found that upon LIPL-4-induced lysosomal lipolysis, a lysosome-to-
277 nucleus retrograde lipid messenger signaling pathway is activated in intestinal cells to promote
278 longevity (Folick et al., 2015; Ramachandran et al., 2019; Savini et al., 2022; Wang et al., 2008).
279 Interestingly, when analyzing the LMP-1 lysosome-enriched proteome in the *lipl-4 Tg* worms,
280 we found an enrichment of nucleus-localized proteins (Figure 4A), including two nucleoporin
281 proteins NPP-6/Nup160 and NPP-15/Nup133 in the Nup160 complex that localizes at the basket
282 side of the nuclear pore (Figure 4B) (Vasu et al., 2001). Such enrichment of nucleoporin proteins
283 was not found in the LMP-1 lysosome-enriched proteome of either WT or the *daf-2(lf)* mutant
284 (Figure 4B). In the cell, mobile lysosomes change their distribution along the perinuclear-
285 peripheral axis in response to different nutrient signals and metabolic status (Ballabio &
286 Bonifacino, 2020; Pu et al., 2016). Moreover, it is known that the cellular position of lysosomes
287 affects their luminal pH, with perinuclear lysosomes being more acidic (Johnson et al., 2016).
288 We found that the lysosome-enriched proteome of the *lipl-4 Tg* worms consists of lysosomal v-
289 ATPase V1 subunits, proton-translocating ATPase and exchanging ion transporters that mediate
290 lysosomal acidification, but these components were not enriched in the WT lysosome proteome
291 (Figure 3B), supporting that lysosomes are more acidic in the *lipl-4 Tg* worms. We thus
292 hypothesize that LIPL-4-induced lysosomal lipolysis may enhance the interaction between
293 lysosomes and the nucleus and further facilitate the lysosome-to-nucleus retrograde lipid
294 signaling to promote longevity.
295
296 To test this hypothesis, we imaged lysosomal positions in intestinal cells where *lipl-4* is
297 expressed. Using a dual reporter strain expressing both lysosomal LMP-1::RFP fusion and
298 nucleus-localized GFP, we found that lysosomes exhibit a dispersed pattern in the intestinal cell

299 of WT worms (Figure 4D). However, in the *lipl-4 Tg* worms, lysosomes are clustered in the
300 perinuclear region (Figure 4D), supporting the hypothesis that the lysosome-nucleus interaction
301 is enhanced. To quantitatively measure this change in lysosomal positioning, we have written an
302 imaging analysis script to analyze the RFP fluorescence signal distribution in intestinal cells
303 (Supplementary Figure 2A). We found the perinuclear and peripheral distribution of lysosomes
304 in the *lipl-4 Tg* worms is significantly increased and decreased, respectively, compared to WT
305 worms ($p<0.01$, Figure 4C, 4D, Supplementary Figure 2B). In contrast, such perinuclear
306 clustering is not observed in intestinal cells of the *daf-2(lf)* mutant (Figure 4E, 4F,
307 Supplementary Figure 2C). Moreover, we found that the RNAi knockdown of *npp-6* suppresses
308 the lifespan extension in the *lipl-4 Tg* worms (Figure 4G, 4H) but does not affect the lifespan
309 extension in the *daf-2(lf)* mutant (Figure 4I, 4J). These results suggest that the enhanced
310 lysosome-nucleus interaction is specifically related to LIPL-4-induced lysosomal signaling and
311 longevity.
312
313 Together, these studies discover changes in the lysosome-enriched proteome between WT and
314 different long-lived strains, and reveal that the lysosomal proteome composition can be
315 influenced by the metabolic status of the lysosome and its interaction with other organelles and
316 in turn correlates with lysosomal signaling and longevity regulation.
317
318 **Profile lysosome-enriched proteome heterogeneity among different tissues**
319
320 Tissue-specific regulation of longevity has been reportedly in various organisms. Next, to
321 examine how lysosome-enriched proteomes exhibit heterogeneity among different tissues, we

322 have generated four transgenic strains that express LMP-1 Lyso-Tag specifically in neurons,
323 muscle, intestine and hypodermis using tissue-specific promoters, *unc-119*, *myo-3*, *ges-1* and
324 *col-12*, respectively (Figure 5A). Using these transgenic strains, we purified lysosomes in a
325 tissue-specific manner and conducted proteomic profiling. The correlation analysis shows good
326 repeatability among three independent biological replicates (Supplementary Figure 3A-D).
327
328 Unlike the whole-body Lyso-IP, the flow-through samples from tissue-specific Lyso-IP contain
329 not only non-lysosomal fractions from the targeted tissue but also lysosomes from non-targeted
330 tissues. Thus, these flow-through samples cannot be simply used as controls to determine the
331 enrichment of proteins at the lysosome in the targeted tissue. To assess tissue-specific changes,
332 we have normalized the level of each identified protein to the level of LMP-1 in the same
333 replicate, and then compared the normalized ratio between the whole-body Lyso-IP and the
334 tissue-specific Lyso-IP (Figure 5B-E, Supplementary Table S5). We found that among the 216
335 proteins identified from the whole-body Lyso-IP, 85 of them show comparable ratios between
336 the whole-body Lyso-IP and the four tissue-specific Lyso-IPs (Figure 5F, Group I), suggesting
337 relative homogenous lysosomal enrichments of these proteins among different tissues. Nine of
338 them were completely absent in the tissue-specific Lyso-IP, which may be related to their low
339 abundance (Figure 5F, Group IV). There are also proteins that were not detected in one or two
340 tissues but exhibited similar enrichments as the whole body Lyso-IP in other tissues, such as
341 PGP-6, an ABC transporter missing in the muscle-specific Lyso-IP, PBO-1, calcium-binding
342 protein P22 missing in the hypodermis-specific Lyso-IP and Y57G11C.33, Golgin A7 missing in
343 both the hypodermis- and neuron-specific Lyso-IPs, which may be associated with their lack of
344 expression and/or lack of lysosome enrichments in specific tissues.

345

346 Importantly, there are 122 proteins that exhibited significant difference in their enrichments
347 between the whole-body Lyso-IP and the tissue-specific Lyso-IPs ($p<0.05$), 56 of them (Group
348 II) showing an increase in the tissue-specific Lyso-IPs while the other 66 (Group III) showing a
349 decrease (Figure 5F). Some of them were only enriched in one tissue but remained unchanged in
350 others, including 15 proteins with higher ratios only in the intestine, 3 only in the hypodermis
351 and 5 only in neurons. There are also five proteins that showed an increased enrichment in one
352 tissue, but a decreased enrichment in another tissue, including AQP-1, an Aquaporin channel
353 with a higher ratio in neurons but a lower one in the hypodermis, Y58A7A.1 a cooper uptake
354 transporter with a higher ratio in the hypodermis but a lower one in the muscle, PBO-4, a
355 sodium/hydrogen exchanger with a higher ratio in the intestine but a lower one in the
356 hypodermis, and two innexin proteins that form gap junctions in invertebrate animals, INX-17
357 with a higher ratio in neurons but a lower ratio in the hypodermis and INX-15 with a higher ratio
358 in the intestine but lower ratios in the muscle and hypodermis (Figure 5F). For these candidates,
359 there is a clear tissue preference with regard to their lysosomal enrichments. Thus, the lysosomal
360 proteome is not only affected by the genotype of the organism, but also exhibits heterogeneity
361 among different tissues within the organism, which may be related to the metabolic status in each
362 tissue and consequently contribute to specific activities and signaling effects of the tissue. Our
363 studies provided a list of candidates for further investigation of the tissue-specific regulation of
364 lysosomal metabolism and signaling.

365

366 **Cystinosin positive mature lysosomes enrich specific lysosomal proteins**

367

368 On the other hand, the analysis of the candidates specifically detected in the *lipl-4 Tg* worms
369 suggest that the proportion of mature lysosomes may also affect the lysosomal protein
370 composition. Although LMP-1 is a well-established lysosomal protein marker and highly
371 abundant on the lysosomal surface, it can be also detected in late endosomes and sometimes in
372 early endocytic compartments. With the hope to profile proteins enriched on mature lysosomes,
373 we chose CTNS-1, the *C. elegans* lysosomal cysteine transporter Cystinosin that is a well-
374 established marker of mature lysosomes (Gahl et al., 1982; Jonas et al., 1982; Kalatzis et al.,
375 2001), and generated a transgenic strain expressing CTNS-1 tagged with both 3×HA and RFP
376 (CTNS-1 *lysoTg*). Fluorescence imaging of RFP confirmed the lysosomal localization of the
377 CTNS-1 fusion protein in live organisms (Figure 6A). Using this transgenic strain, we followed
378 the same Lyso-IP and MS profiling approaches. The correlation analysis shows good
379 repeatability among three independent biological replicates (Supplementary Figure 1G), and the
380 PCA analysis indicates a clear separation between Lyso-IP samples and flow-through controls
381 (Supplementary Figure 1F). Using the same selection criteria, we identified 293 candidates
382 whose levels are enriched at least 10-fold in the purified lysosomes than those in the flow-
383 through controls among all independent biological replicates and show over 2-fold enrichment
384 compared to the non-tag controls (Supplementary Table 6). There are 95 lysosome-enriched
385 proteins shared between the LMP-1 and the CTNS-1 Lyso-IP proteomic profiling datasets
386 (Figure 6B, Supplementary Table 6), and 47 of these shared proteins are annotated with
387 lysosomal localization (Supplementary Table 6). We have also crossed the CTNS-1 *lysoTg* strain
388 with the *lipl-4 Tg* strain and the *daf-2(lf)* mutant and then conducted Lyso-IP proteomic
389 profiling. However, the pull-down efficiency was very low in these long-lived worms, which
390 prevents us to identify proteins unique to CTNS-1 Lyso-IP in those conditions.

391

392 In WT worms, the proportions of the identified proteins with different categories of subcellular
393 annotation are comparable between LMP-1 and CTNS-1 Lyso-IP conditions (Figure 6C, 2E),
394 and for proteins with lysosomal annotation, the proportion is 25% and 28% in LMP-1 and
395 CTNS-1 Lyso-IP, respectively (Figure 6D). However, among the 121 proteins only identified in
396 LMP-1 Lyso-IP, there are only 8 with lysosomal annotation (7%); while for the 198 proteins
397 only identified in CTNS-1 Lyso-IP, 35 are with lysosomal annotation and the proportion remains
398 as 18% (Figure 6D). Among the lysosomal proteins that are unique to CTNS-1 Lyso-IP, there are
399 autophagosome proteins and proteins that mediate the fusion between autophagosomes and
400 lysosomes, including ATG-9/ATG9A (Popovic & Dikic, 2014), C33A11.2/DRAM2 (Crighton et
401 al., 2006), EPG-7/RB1CC1 (Nishimura et al., 2013), and VAMP-7/VAMP8 (Diao et al., 2015;
402 Itakura et al., 2012) (Figure 6E). CTNS-1 Lyso-IP unique candidates also include the Ragulator
403 complex components LMTR-2/3/5, the lysosomal amino acid transporter F13H10.3/SLC38A9
404 and the lysosomal calcium channel CUP-5/TRPML1 that regulate mTORC1 signaling (Li et al.,
405 2016; Rebsamen et al., 2015; Wang et al., 2015; Wyant et al., 2017) (Figure 6E). These results
406 suggest that CTNS-1 Lyso-IP enriches lysosomes that are actively involved in autophagy and
407 transduce mTORC1 signaling.

408

409 Furthermore, when systemically examining 85 lysosome-related proteins that were previously
410 annotated in *C. elegans* based on sequence homology (Sun et al., 2020), we found that many
411 lysosomal hydrolases exhibit increased enrichments with CTNS-1 Lyso-IP, especially for those
412 cysteine proteases including CPR-6, LGMN-1, CPL-1, CPZ-1 and TAG-196 (Figure 6F). These
413 enrichments are consistent with that CTNS-1 is located at mature lysosomes as a cysteine

414 transporter (Gahl et al., 1982; Jonas et al., 1982; Kalatzis et al., 2001). The similar increased
415 enrichments of lysosomal hydrolases were also observed in the LMP-1 Lyso-IP candidates
416 identified from the *lipl-4 Tg* worms (Figure 6F), further supporting that the long-lived *lipl-4 Tg*
417 worms carry more acidic lysosomes. Together, we found that lysosome-enriched proteomes
418 identified from both LMP-1 and CTNS-1 Lyso-IP consist of well-characterized lysosomal
419 enzymes and integral membrane proteins as well as proteins that contribute to lysosomal
420 signaling, dynamics and contact with other cellular compartments. Besides many known
421 lysosomal proteins, various proteins that are not previously linked with lysosomes are now
422 identified through these systemic analyses.
423
424 **Lysosome-enriched proteins regulate different lysosomal activities**
425
426 To understand the role of these newly identified lysosome-enriched proteins in regulating
427 lysosomal functions, we have examined their effects on lysosomes using an RNAi screen based
428 on LysoSensor fluorescence intensity. We focused on 95 lysosome-enriched proteins shared
429 between LMP-1 and CTNS-1 Lyso-IPs and knocked down their coding genes by RNAi, and then
430 used LysoSensor probes to stain lysosomes. From screening these 95 candidates (Supplementary
431 Table 7), we have identified five genes whose inactivation cause changes in LysoSensor signal
432 intensity, and four of them have human homologs, including two lysosomal v-ATPase subunits,
433 UNC-32/ATP6V0A and VHA-5/ATP6V0A, the lysosomal amino acid transporter SLC-
434 36.2/SLC36A1 (SLC36A4), and a transmembrane protein R144.6/TMEM144 (Supplementary
435 Table 7, Supplementary Figure 5). We further examined their effects on the lysosomal number,
436 size and pH. We found that the RNAi knockdown of the two lysosomal v-ATPase subunits,

437 UNC-32 and VHA-5, lead to decreased lysosomal numbers (Figure 7F), but an increase in the
438 lysosomal size (Figure 7G). Using fluorescence lifetime microscopy, we also found that the
439 RNAi knockdown of R144.6 and UNC-32 increases and decreases lysosomal pH, respectively
440 (Figure 7H).
441
442 UNC-32, VHA-5 and SLC-36.2 are well-known lysosomal proteins, but the subcellular
443 localization of the R144.6 protein remains unknown. R144.6 is a predicted carbohydrate
444 transporter, and structural simulation using AlphaFold2 revealed it as a solute carrier family
445 (SLC) transporter (Figure 7I). To characterize its subcellular localization, we have generated a
446 CRISPR knock-in line in which the endogenous R144.6 protein is fused with the fluorescent
447 protein NeonGreen and then stained these worms with LysoTracker Red to mark lysosomes. In
448 the hypodermis, we found that NeonGreen and LysoTracker Red signals overlap, confirming the
449 lysosomal localization of this newly identified transmembrane protein from Lyso-IP (Figure 7J).
450 On the other hand, its expression was not detected in the muscle, and in the intestine, its
451 NeonGreen signals were not overlapped with LysoTracker Red, which is consistent with tissue-
452 specific Lyso-IP analyses. R144.6 were enriched in the hypodermis-specific Lyso-IP at a similar
453 level as in the whole-body Lyso-IP; however, it was not detected in the muscle- or intestine-
454 specific Lyso-IP (Supplementary Table 5). These results further support the enrichment
455 specificity of proteins at the lysosome in different tissues as well as the power of the Lyso-IP
456 proteomic profiling in discovering new lysosomal proteins with functional significance.
457
458 **DISCUSSION**
459

460 In summary, our studies reveal the heterogeneity of lysosomal protein composition that is
461 associated with lysosomal status, tissue specificity, and organism longevity. Through systemic
462 profiling of lysosome-enriched proteins under different conditions, we confirmed the induction
463 of lysosome-related autophagy by different longevity-promoting pathways, unveiled increased
464 cellular interaction between lysosomes and the nucleus upon the induction of lysosomal lipolysis
465 and its contribution to longevity regulation, and underlined the importance of the spatial control
466 of AMPK activation in regulating longevity. Our studies provide not only methods for future
467 studies to profile the dynamics of the lysosomal proteome in response to diverse physiological
468 inputs, but also resources for understanding the vital contribution of these dynamics in
469 modulating signal transduction, organelle crosstalk and organism longevity.
470
471 These proteomic studies reveal changes in the interaction between lysosomes and other
472 organelles under different conditions. One example is lysosome-nucleus interaction. In the Lyso-
473 IP fraction from WT worms, we did not detect any proteins with sole nuclear localization;
474 however, in the Lyso-IP fraction from the *lipl-4 Tg* or *daf-2(lf)* mutant worms, nuclear proteins
475 were identified and the percentage of the increase over WT is significantly higher in the *lipl-4 Tg*
476 worms ($p<0.05$, Figure 4A, Supplementary Figure 4). Based on this finding, we discovered the
477 previously unknown perinuclear accumulation of lysosomes in the *lipl-4 Tg* worms (Figure 4C,
478 4D) and further confirmed its importance for longevity regulation (Figure 4G, 4H). It is shown
479 previously that perinuclear lysosomes are more acidic than peripheral lysosomes (Johnson et al.,
480 2016; Webb et al., 2021). Thus, the increase in perinuclear lysosomes may be associated with the
481 increased proportion of mature lysosomes in the *lipl-4 Tg* worms, which is supported by the
482 increased enrichments of lysosomal v-ATPase, channels/transporters and hydrolases (Figure 3B).

483 This increased distribution of lysosomes toward the perinuclear region could facilitate proteins
484 and metabolites transporting from the lysosome to the nucleus through the nuclear pore and in
485 turn their signaling effects. On the other hand, we did not detect perinuclear accumulation of
486 lysosomes in the *daf-2(lf)* mutant worms by cellular imaging, and the nuclear proteins detected
487 through LMP-1 Lyso-IP from the *daf-2(lf)* mutant worms are mainly involved in RNA splicing.
488 In yeast cells, defects in pre-RNA processing have been associated with nucleophagy (Leger-
489 Silvestre et al., 2005) that involves SQSTM1 and lysosomes (Ivanov et al., 2013; Mijaljica &
490 Devenish, 2013). We thus speculate that the increased enrichment of nuclear proteins in the *daf-*
491 *2(lf)* mutant worms may be associated with the induction of nucleophagy but not changes in
492 lysosomal positioning.
493
494 mTORC1 and AMPK are key metabolic checkpoints that regulate anabolic and catabolic
495 processes in mutually opposing ways. In sensing the lack of nutrients, AMPK signals activate the
496 catabolic process while inhibiting the anabolic one. On the other hand, responding to nutrient
497 availability, mTORC1 activation upregulates anabolic metabolism and promotes cell growth.
498 Intriguingly, it is now known that both mTORC1 and AMPK are recruited to the lysosomal
499 surface for activation, which requires the scaffold Ragulator complex that consists of LAMTOR
500 subunits. We found that the Ragulator complex (LMTR-2, 3 and 5) is enriched at the lysosome
501 purified from WT worms using CTNS-1 but not LMP-1 Lyso-IP (Figure 6E), suggesting a
502 predominant association of the Ragulator complex with mature lysosomes, which could in turn
503 determine the preference of mTORC1 and AMPK activation at the lysosomal surface.
504 Alternatively, it would be also possible that the Ragulator complex carries a preference toward
505 CTNS-1/Cystinosin-containing lysosomes, which would infer the interaction between lysosomal

506 cysteine metabolism and mTORC1 signaling. Interestingly, previous studies show that
507 Cystinosin co-immunoprecipitates with the Ragulator complex in mammalian cells
508 (Andrzejewska et al., 2016), and in *Drosophila,* cysteine efflux from the lysosome via Cystinosin
509 antagonizes mTORC1 signaling and upregulates the tricarboxylic acid cycle (Jouandin et al.,
510 2022). Whether this inhibitory effect of lysosomal cysteine on mTORC1 is related to the
511 preferential interaction between the Ragulator complex and Cystinosin would be an interesting
512 question for future studies.
513
514 Both mTORC1 and AMPK have been implicated in the regulation of longevity across different
515 species, being intertwined with other longevity regulatory mechanisms (Savini et al., 2019). In
516 the long-lived *lipl-4 Tg* worms, the lysosomal enrichment of the Ragulator complex is increased
517 with LMP-1 Lyso-IP, which may be a result of the increased proportion of mature lysosomes
518 upon the induction of lysosomal lipolysis. At the same time, we could not rule out the possibility
519 that the increased enrichment of the Ragulator complex is a result of the induced level of
520 lysosomal CTNS-1/Cystinosin in the *lipl-4 Tg* worms. We found that with LMP-1 Lyso-IP, the
521 level of the CTNS-1/Cystinosin transporter is increased in the *lipl-4 Tg* worms, together with the
522 increase of several cysteine cathepsins (Figure 6F). Our previous studies found that
523 mitochondrial β-oxidation is increased in the *lipl-4 Tg* worms, leading to decreased triglyceride
524 storage (Ramachandran et al., 2019). The *lipl-4 Tg* worms also show an induced autophagy (Mak
525 et al., 2020). These phenotypes are the same as those observed in fruit flies with Cystinosin
526 overexpression (Jouandin et al., 2022). Considering the inhibitory effect of Cystinosin on
527 mTORC1 in fruit flies, the induction of Cystinosin in the *lipl-4 Tg* worms might reduce
528 mTORC1 signaling. In supporting this idea, our unpublished study shows that *lipl-4 Tg* does not

529 further enhance the lifespan extension of the *raga-1* mutant that has reduced mTORC1 signaling.
530 Furthermore, our study reveals the lysosomal enrichment of AMPK in the *lipl-4 Tg* worms, and
531 its requirement for the longevity effect (Figure 3C, 3D). On the other hand, the involvement of
532 lysosomal mTORC1 and AMPK signaling in regulating the longevity effect associated with
533 reduced insulin/IGF-1 signaling was not identified in the *daf-2(lf)* mutant. It would be interesting
534 for future studies to systemically profile lysosome-enriched proteomes in other longevity models,
535 such as caloric restriction, mild inhibition of mitochondrial respiration and germline deficiency,
536 using the same method, which would help understand the involvement of lysosomal metabolism
537 and signaling in these different longevity mechanisms.
538

539 **MATERIALS AND METHODS**

540

541 ***C. elegans* strains and maintenance**

542 The following strains were used in this study: N2, CB1370 *daf-2(e1370),* RB754 *aak-2(ok524)*,
543 *unc-76(e911)*, MCW953 *nre-1(hd20);lin-15b(hd126)*, MCW14 *raxIs3 [ges-1p::lipl-*
544 *4::SL2GFP]*, MCW859 *raxIs103[sur-5p:lmp-1::RFP-3×HA;unc-76(+)],* MCW935 *daf-*
545 *2(e1370);raxIs103[sur-5p:lmp-1::RFP-3×HA;unc-76(+)],* MCW923 *raxIs3[ges-1p::lipl-*
546 *4::SL2GFP];raxIs103[sur-5p:lmp-1::RFP-3×HA;unc-76(+)], MCW861 unc-*
547 *76(e911);raxEx311[Pmyo-3:lmp-1::RFP-3×HA;unc-76(+)],* MCW924 *unc-76(e911);*
548 *raxEx346[Pcol-12:lmp-1::RFP-3×HA;unc-76(+)],* MCW862 *unc-76(e911);raxEx312[Punc-*
549 *119:lmp-1::RFP-3×HA;unc-76(+)],* MCW914 *unc-76(e911);raxEx341[Pges-1:lmp-1::RFP-*
550 *3×HA;unc-76(+)],* MCW934 *raxIs118[sur-5p:ctns-1::RFP-3×HA;unc-76(+)].* The strains N2,

551 CB1370, and RB754 were obtained from *Caenorhabditis* Genetics Center (CGC). The strain
552 *unc-76(e911)* was obtained from Dr. Zheng Zhou's Lab. Other strains were generated in our lab.
553
554 *C. elegans* strains were maintained at 20˚C on standard NGM agar plates seeded with OP50
555 *E.coli* (HT115 *E. coli* for RNAi experiments) using standard protocols (Stiernagle, 2006) and
556 kept at least three generations without starvation before experiments.
557
558 **Molecular cloning and generating transgenics**
559 All the expression constructs were generated using Multisite Gateway System (Invitrogen) as
560 previously described (Mutlu et al., 2020). The *lmp-1* and *ctns-1* coding sequences were PCR-
561 amplified from *C. elegans* cDNA then inframe fused with RFP-3×HA, and all promoters were
562 PCR-amplified from *C. elegans* genomic DNA.
563
564 Transgenic strains were generated by microinjecting the day-1-adult germline of *unc-76(e911)*
565 worms with DNA mixture containing expression construct and *unc-76(+)* rescuing plasmid. For
566 integration strains, the stable extrachromosomal arrays were integrated with gamma irradiation
567 (4500 rads for in 5.9 minutes) and backcrossing to wild-type N2 at least 8 times.
568
569 **Lysosome immunoprecipitation (Lyso-IP)**
570 Lyso-IP is based on the method used in mammalian cells (Abu-Remaileh et al., 2017). Briefly,
571 transgenic strains stably expressing C-terminal RFP- and 3×HA-tagged lysosomal membrane
572 protein LMP-1 or CTNS-1 under whole-body *Psur-5* or tissue-specific promoters were
573 generated. Around 160,000 day-1-adult worms per genotype were collected, washed 3 times with

574 M9 buffer then washed 1 time with KPBS buffer (136 mM KCl, 10 mM KH_2PO_4). Worms in 2
575 ml KPBS were quickly homogenized with Dounce homogenizer on ice until no visible animals
576 were seen under the microscope. The lysate was centrifuged at 1000 g for 3 min at 4 ˚C to
577 remove debris and then the supernatant was incubated with anti-HA magnetic beads (Thermo
578 Fisher Scientific, cat. # 88837) for 6 minutes at 20 ˚C. The bound beads and flowthrough were
579 separated using a magnetic stand. The bound bead fraction was washed 4 times with cold KPBS.
580 The bound bead and flowthrough fractions were both used for LC/MS-based proteomics
581 analyses.
582
583 **LC/MS-based proteomic analyses**
584 The bound beads after wash were directly eluted in 100 µl of 5% SDS buffer and trypsin
585 digestion was carried out using S-Trap™ (Protifi, NY) as per manufacturer's protocol. For the
586 flow-through sample after IP, 100 µl sample was diluted in 5% SDS buffer and trypsin digestion
587 was carried out using S-Trap™. The peptide concentration was measured using the Pierce™
588 Quantitative Colorimetric Peptide Assay (Thermo Scientific cat. # 23275). The digested peptides
589 were subjected to simple C18 clean up using a C18 disk plug (3M Empore C18) and dried in a
590 speed vac. 1 µg of the peptide was used for LC-MS/MS analysis which was carried out using a
591 nano-LC 1200 system (Thermo Fisher Scientific, San Jose, CA) coupled to Orbitrap Fusion™
592 Lumos ETD mass spectrometer (Thermo Fisher Scientific, San Jose, CA). The peptides were
593 loaded on a two-column setup using a pre-column trap of 2 cm × 100 µm size (Reprosil-Pur
594 Basic C18 1.9 µm, Dr. Maisch GmbH, Germany) and a 5 cm × 75 µm analytical column
595 (Reprosil-Pur Basic C18 1.9 µm, Dr. Maisch GmbH, Germany) with a 75 min gradient of 5-28%
596 acetonitrile/0.1% formic acid at a flow rate of 750 nl/min. The eluted peptides were directly

597 electro-sprayed into mass spectrometer operated in the data-dependent acquisition (DDA) mode.
598 The full MS scan was acquired in Orbitrap in the range of 300-1400 m/z at 120,000 resolution
599 followed by top 30 MS2 in Ion Trap (AGC 5000, MaxIT 35 ms, HCD 28% collision energy)
600 with 15 sec dynamic exclusion time.
601
602 The raw files were searched using Mascot algorithm (Mascot 2.4, Matrix Science) against the
603 *Caenorhabditis elegans* NCBI refseq protein database in the Proteome Discoverer (PD 2.1,
604 Thermo Fisher) interface. The precursor mass tolerance was set to 20 ppm, fragment mass
605 tolerance to 0.5 Da, maximum of two missed cleavage was allowed. Dynamic modification of
606 oxidation on methionine, protein N-terminal Acetylation and deamidation (N/Q) was allowed.
607 The gene product inference and iBAQ-based quantification were carried out using the gpGrouper
608 algorithm (Saltzman et al., 2018). The iBAQ values were normalized to the fraction of total
609 protein iBAQ per experiment defined as 'iFOT (Fraction of total)'.
610
611 **Antibodies**
612 Anti-*C. elegans* LMP-1, HSP-60, β-actin, CYP-33, SVQ-8 monoclonal antibodies were
613 purchased from Developmental Studies Hybridoma Bank (DHSB). Those antibodies were
614 originally generated by Dr. Michael L. Nonet's lab (Hadwiger et al., 2010).
615
616 **Microscopy imaging**
617 <u>Regular microscopy</u>
618 Tissue-specific lyso-Tag expression example images (Figure 5A) were captured using Leica
619 DMi8 THUNDER Imaging Systems using 20× objective. Other microscopy images were

620 captured using Olympus FV3000 confocal microscopy system using 60× or 20× objective. *C.*
621 *elegans* were anesthetized in 1% sodium azide in M9 buffer and placed on 2% agarose pad
622 sandwiched between the glass microscopic slide and coverslip.
623
624 Fluorescence lifetime microscopy
625 L1 RNAi sensitive *nre-1(hd20);lin-15b(hd126)* worms were seeded on 3.5cm RNAi plates and
626 raised at 20°C for two days, and then around 20 worms each well were transferred to the 3.5cm
627 RNAi plates containing RNAi bacteria and 0.5 μM of LysoSensor Green DND-189
628 (Invitrogen™ L7535) and raised for 18h (in dark) at 20°C. The worms were imaged using ISS
629 Q2 Time-resolved Laser Scanning Confocal Nanoscope. The laser excitation wavelength was set
630 at 476nm and the 500-633nm emission filter was used to detect the LysoSenor Green signal. The
631 first pair of intestinal cells of each worm was imaged. The lifetimes of LysoSensor-containing
632 puncta were measured using ISS VistaVision software. The pH of the lysosome was then
633 calculated based on the LysoSensor lifetime-pH calibration curve.
634
635 **LysoSensor RNAi screen**
636 The primary screen was performed on 95 lysosomal-enriched candidates shared between the
637 LMP-1 and the CTNS-1 Lyso-IP proteomic profiling datasets. Each RNAi bacteria clone was
638 seeded onto 12-well RNAi plates containing 1 mM IPTG and allowed to dry. The dried plates
639 were then incubated at room temperature overnight to induce dsRNA expression. Synchronized
640 L1 *nre-1(hd20);lin-15b(hd126)* worms were seeded on 12-well RNAi plates and raised at 20 °C
641 for two days, and then around 30 worms each well were transferred to the RNAi plates
642 containing RNAi bacteria and 0.5 μM of LysoSensor Green DND-189. After 18 hours,

643 LysoSensor signals were examined by naked eyes using Nikon SMZ18 fluorescence stereo
644 microscope. The candidates with obvious LysoSensor alteration were selected for the secondary
645 LysosSensor RNAi screen. In the secondary screen, worms stained using LysoSensor Green
646 DND-189 were imaged by the FV3000 confocal laser scanning microscope (At least 15 animals
647 were measured in each condition). The changes in LysoSensor signals in the first pair of intestine
648 cells were quantified by ImageJ (including intensity, size, and number).
649

650 **Lysosome distribution quantification**

651 The quantification method was modified from previous publications on lysosomal distribution in
652 mammalian cell lines (Johnson et al., 2016; Willett et al., 2017). Images were first captured using
653 Olympus Fluoview software and imported into Matlab by Bio-Formats tool (Linkert et al., 2010).
654 Next, the cell membrane and nuclear membrane are outlined manually. The algorithm (codes
655 included in Supplementary materials) determines the geometric center of the nucleus and radiates
656 at all angles to locate line segments between the nuclear and cell membrane. The line segments
657 are then evenly divided and circled to segment the cytosol into different regions. We calculate: 1.
658 The mean RFP fluorescence distribution across regions (normalized to the mean intensity of the
659 whole cell to avoid variations of RFP expression across cells) (Figure 4D, 4F); 2. The cumulative
660 intensity distribution from the most perinuclear region to the most peripheral region (normalized
661 to the overall intensity of the whole cell) (Supplementary Figure 2B, 2C). The algorithm requires
662 a convex shape of the cell, and most of the gut cells imaged meet this need.
663

664 **Lifespan assays**

665 Worms were synchronized by bleach-based egg preparation and subsequent starvation in M9
666 buffer for over 24 hours. Synchronized L1 worms were placed on the plates, and animals were
667 synchronized again by manual picking at mid L4 stage and marked as Day 0. Approximately 90-
668 120 worms were placed in three parallel plates for each condition. Worms are hence observed
669 and transferred to freshly made RNAi plates every other day. Animals are categorized as alive,
670 death (cessation of movement in response to platinum wire probing) or censored. The statistical
671 analyses were performed with the SPSS23 Kaplan-Meier survival function and the log-rank test.
672 GraphPad Prism 9 was used to graph the results.
673

674 **Structural stimulation by AlphaFold2**

675 The structure of R144.6 (UniProt: Q10000) was predicted by AlphaFold2 and downloaded from
676 The AlphaFold Protein Structure Database (https://alphafold.ebi.ac.uk/) (Jumper et al., 2021;
677 Varadi et al., 2022). The molecular graphics of the R144.6 structure was performed with UCSF
678 Chimera (Pettersen et al., 2004).
679

680 **Statistical methods**

681 Principal components analysis (PCA) was performed by R package Factextra (Le et al., 2008)
682 with the normalized iFOT abundance of proteins detected as the input. The Pearson correlation
683 matrices and coefficient (r) among replicates were generated by GraphPad Prism 9. The
684 unpaired, two-tailed t-tests for the multiple comparisons were used to calculate the p-values in
685 the correlation analyses by GraphPad Prism 9.
686

687 **ACKNOWLEDGEMENTS**

688 We thank A. Dervisefendic and P. Svay for maintenance support; Mass Spectrometry Proteomics
689 Core of Baylor College of Medicine for mass spectrometry proteomic analysis; Z. Zhou (Baylor
690 College of Medicine) for sharing *unc-76(e911)* strain. Some strains were obtained from the
691 *Caenorhabditis* Genetics Center (CGC), which is funded by NIH Office of Research
692 Infrastructure Programs (P40 OD010440). M.C.W. is currently supported by Howard Hughes
693 Medical Institute, and Y.Y. is currently supported by National Natural Science Foundation of
694 China 32071146.

695

696 **AUTHOR CONTRIBUTIONS**

697 Y.Y., S.M.G., Y.G. and M.C.W. conceived the project and designed the experiments. Y.Y.,
698 S.M.G., Y.G., P.H., Q. Zhang, J.L., B.J. and S.Y.J. performed experiments. Q. Zhao conducted
699 the structural simulation. D.M.S. and M.A. help design Lyso-IP method in *C. elegans*. S.Y.J.
700 supervised mass spectrometry analysis. Y.Y., S.M.G., Y.G. and M.C.W. wrote the manuscript.
701 Y.Y., S.M.G., Y.G., Q. Zhang, M.A. and M.C.W. edited the manuscript.

702

703 **COMPETING INTERESTS**

704 The authors declare no competing interests.

705

706 **REFERENCE**

707

708 Abu-Remaileh, M., Wyant, G. A., Kim, C., Laqtom, N. N., Abbasi, M., Chan, S. H., Freinkman, E.,
709 & Sabatini, D. M. (2017). Lysosomal metabolomics reveals V-ATPase- and mTOR-

710 dependent regulation of amino acid efflux from lysosomes. *Science*, *358*(6364), 807-813.
711 https://doi.org/10.1126/science.aan6298
712 Andrzejewska, Z., Nevo, N., Thomas, L., Chhuon, C., Bailleux, A., Chauvet, V., Courtoy, P. J., Chol,
713 M., Guerrera, I. C., & Antignac, C. (2016). Cystinosin is a Component of the Vacuolar H+-
714 ATPase-Ragulator-Rag Complex Controlling Mammalian Target of Rapamycin Complex 1
715 Signaling. *J Am Soc Nephrol*, *27*(6), 1678-1688.
716 https://doi.org/10.1681/ASN.2014090937
717 Apfeld, J., O'Connor, G., McDonagh, T., DiStefano, P. S., & Curtis, R. (2004). The AMP-activated
718 protein kinase AAK-2 links energy levels and insulin-like signals to lifespan in *C. elegans*.
719 *Genes Dev*, *18*(24), 3004-3009. https://doi.org/10.1101/gad.1255404
720 Appelqvist, H., Waster, P., Kagedal, K., & Ollinger, K. (2013). The lysosome: from waste bag to
721 potential therapeutic target. *J Mol Cell Biol*, *5*(4), 214-226.
722 https://doi.org/10.1093/jmcb/mjt022
723 Ballabio, A., & Bonifacino, J. S. (2020). Lysosomes as dynamic regulators of cell and organismal
724 homeostasis. *Nature reviews Molecular cell biology*, *21*(2), 101-118.
725 https://doi.org/10.1038/s41580-019-0185-4
726 Ballabio, A., & Gieselmann, V. (2009). Lysosomal disorders: from storage to cellular damage.
727 *Biochim Biophys Acta*, *1793*(4), 684-696. https://doi.org/10.1016/j.bbamcr.2008.12.001
728 Braulke, T., & Bonifacino, J. S. (2009). Sorting of lysosomal proteins. *Biochimica Et Biophysica*
729 *Acta-Molecular Cell Research*, *1793*(4), 605-614.
730 https://doi.org/10.1016/j.bbamcr.2008.10.016

731 Brown, C. A., & Black, S. D. (1989). Membrane topology of mammalian cytochromes P-450 from
732 liver endoplasmic reticulum. Determination by trypsinolysis of phenobarbital-treated
733 microsomes. *J Biol Chem*, *264*(8), 4442-4449.
734 https://www.ncbi.nlm.nih.gov/pubmed/2925650
735 Castellano, B. M., Thelen, A. M., Moldavski, O., Feltes, M., van der Welle, R. E., Mydock-
736 McGrane, L., Jiang, X., van Eijkeren, R. J., Davis, O. B., Louie, S. M., Perera, R. M., Covey,
737 D. F., Nomura, D. K., Ory, D. S., & Zoncu, R. (2017). Lysosomal cholesterol activates
738 mTORC1 via an SLC38A9-Niemann-Pick C1 signaling complex. *Science*, *355*(6331), 1306-
739 1311. https://doi.org/10.1126/science.aag1417
740 Crighton, D., Wilkinson, S., O'Prey, J., Syed, N., Smith, P., Harrison, P. R., Gasco, M., Garrone, O.,
741 Crook, T., & Ryan, K. M. (2006). DRAM, a p53-induced modulator of autophagy, is critical
742 for apoptosis. *Cell*, *126*(1), 121-134. https://doi.org/10.1016/j.cell.2006.05.034
743 Cruciat, C. M., Ohkawara, B., Acebron, S. P., Karaulanov, E., Reinhard, C., Ingelfinger, D.,
744 Boutros, M., & Niehrs, C. (2010). Requirement of prorenin receptor and vacuolar H+-
745 ATPase-mediated acidification for Wnt signaling. *Science*, *327*(5964), 459-463.
746 https://doi.org/10.1126/science.1179802
747 Davidson, S. M., & Vander Heiden, M. G. (2017). Critical Functions of the Lysosome in Cancer
748 Biology. *Annu Rev Pharmacol Toxicol*, *57*, 481-507. https://doi.org/10.1146/annurev-
749 pharmtox-010715-103101
750 de Araujo, M. E. G., Naschberger, A., Furnrohr, B. G., Stasyk, T., Dunzendorfer-Matt, T., Lechner,
751 S., Welti, S., Kremser, L., Shivalingaiah, G., Offterdinger, M., Lindner, H. H., Huber, L. A.,
752 & Scheffzek, K. (2017). Crystal structure of the human lysosomal mTORC1 scaffold

753 complex and its impact on signaling. *Science*, *358*(6361), 377-381.
754 https://doi.org/10.1126/science.aao1583
755 De Franceschi, N., Hamidi, H., Alanko, J., Sahgal, P., & Ivaska, J. (2015). Integrin traffic - the
756 update. *J Cell Sci*, *128*(5), 839-852. https://doi.org/10.1242/jcs.161653
757 Diao, J., Liu, R., Rong, Y., Zhao, M., Zhang, J., Lai, Y., Zhou, Q., Wilz, L. M., Li, J., Vivona, S.,
758 Pfuetzner, R. A., Brunger, A. T., & Zhong, Q. (2015). ATG14 promotes membrane
759 tethering and fusion of autophagosomes to endolysosomes. *Nature*, *520*(7548), 563-
760 566. https://doi.org/10.1038/nature14147
761 Eapen, V. V., Swarup, S., Hoyer, M. J., Paulo, J. A., & Harper, J. W. (2021). Quantitative
762 proteomics reveals the selectivity of ubiquitin-binding autophagy receptors in the
763 turnover of damaged lysosomes by lysophagy. *Elife*, *10*.
764 https://doi.org/10.7554/eLife.72328
765 Eskelinen, E. L. (2006). Roles of LAMP-1 and LAMP-2 in lysosome biogenesis and autophagy.
766 *Mol Aspects Med*, *27*(5-6), 495-502. https://doi.org/10.1016/j.mam.2006.08.005
767 Ewan, L. C., Jopling, H. M., Jia, H. Y., Mittar, S., Bagherzadeh, A., Howell, G. J., Walker, J. H.,
768 Zachary, I. C., & Ponnambalam, S. (2006). Intrinsic tyrosine kinase activity is required for
769 vascular endothelial growth factor receptor 2 ubiquitination, sorting and degradation in
770 endothelial cells. *Traffic*, *7*(9), 1270-1282. https://doi.org/10.1111/j.1600-
771 0854.2006.00462.x
772 Fehrenbacher, N., & Jaattela, M. (2005). Lysosomes as targets for cancer therapy. *Cancer Res*,
773 *65*(8), 2993-2995. https://doi.org/10.1158/0008-5472.CAN-05-0476

774 Folick, A., Oakley, H. D., Yu, Y., Armstrong, E. H., Kumari, M., Sanor, L., Moore, D. D., Ortlund, E.
775 A., Zechner, R., & Wang, M. C. (2015). Lysosomal signaling molecules regulate longevity
776 in *Caenorhabditis elegans*. *Science*, *347*(6217), 83-86.
777 https://doi.org/10.1126/science.1258857
778 Forgac, M. (2007). Vacuolar ATPases: rotary proton pumps in physiology and pathophysiology.
779 *Nat Rev Mol Cell Biol*, *8*(11), 917-929. https://doi.org/10.1038/nrm2272
780 Gahl, W. A., Bashan, N., Tietze, F., Bernardini, I., & Schulman, J. D. (1982). Cystine transport is
781 defective in isolated leukocyte lysosomes from patients with cystinosis. *Science*,
782 *217*(4566), 1263-1265. https://doi.org/10.1126/science.7112129
783 Gallet, A., & Therond, P. P. (2005). Temporal modulation of the Hedgehog morphogen gradient
784 by a patched-dependent targeting to lysosomal compartment. *Developmental Biology*,
785 *277*(1), 51-62. https://doi.org/10.1016/j.ydbio.2004.09.005
786 Gao, Y., Chen, Y., Zhan, S., Zhang, W., Xiong, F., & Ge, W. (2017). Comprehensive proteome
787 analysis of lysosomes reveals the diverse function of macrophages in immune
788 responses. *Oncotarget*, *8*(5), 7420-7440. https://doi.org/10.18632/oncotarget.14558
789 Grant, B., & Hirsh, D. (1999). Receptor-mediated endocytosis in the *Caenorhabditis elegans*
790 oocyte. *Mol Biol Cell*, *10*(12), 4311-4326. https://doi.org/10.1091/mbc.10.12.4311
791 Graves, A. R., Curran, P. K., Smith, C. L., & Mindell, J. A. (2008). The Cl-/H+ antiporter ClC-7 is the
792 primary chloride permeation pathway in lysosomes. *Nature*, *453*(7196), 788-792.
793 https://doi.org/10.1038/nature06907
794 Hadwiger, G., Dour, S., Arur, S., Fox, P., & Nonet, M. L. (2010). A monoclonal antibody toolkit for
795 *C. elegans*. *PLoS One*, *5*(4), e10161. https://doi.org/10.1371/journal.pone.0010161

796 Hansen, M., Rubinsztein, D. C., & Walker, D. W. (2018). Autophagy as a promoter of longevity:
797 insights from model organisms. *Nat Rev Mol Cell Biol*, *19*(9), 579-593.
798 https://doi.org/10.1038/s41580-018-0033-y
799 Hartl, F. U., Martin, J., & Neupert, W. (1992). Protein folding in the cell: the role of molecular
800 chaperones Hsp70 and Hsp60. *Annu Rev Biophys Biomol Struct*, *21*, 293-322.
801 https://doi.org/10.1146/annurev.bb.21.060192.001453
802 Itakura, E., Kishi-Itakura, C., & Mizushima, N. (2012). The hairpin-type tail-anchored SNARE
803 syntaxin 17 targets to autophagosomes for fusion with endosomes/lysosomes. *Cell*,
804 *151*(6), 1256-1269. https://doi.org/10.1016/j.cell.2012.11.001
805 Ivanov, A., Pawlikowski, J., Manoharan, I., van Tuyn, J., Nelson, D. M., Rai, T. S., Shah, P. P.,
806 Hewitt, G., Korolchuk, V. I., Passos, J. F., Wu, H., Berger, S. L., & Adams, P. D. (2013).
807 Lysosome-mediated processing of chromatin in senescence. *J Cell Biol*, *202*(1), 129-143.
808 https://doi.org/10.1083/jcb.201212110
809 Johnson, D. E., Ostrowski, P., Jaumouille, V., & Grinstein, S. (2016). The position of lysosomes
810 within the cell determines their luminal pH. *J Cell Biol*, *212*(6), 677-692.
811 https://doi.org/10.1083/jcb.201507112
812 Jonas, A. J., Greene, A. A., Smith, M. L., & Schneider, J. A. (1982). Cystine accumulation and loss
813 in normal, heterozygous, and cystinotic fibroblasts. *Proc Natl Acad Sci U S A*, *79*(14),
814 4442-4445. https://doi.org/10.1073/pnas.79.14.4442
815 Jouandin, P., Marelja, Z., Shih, Y. H., Parkhitko, A. A., Dambowsky, M., Asara, J. M., Nemazanyy,
816 I., Dibble, C. C., Simons, M., & Perrimon, N. (2022). Lysosomal cystine mobilization

817 shapes the response of TORC1 and tissue growth to fasting. *Science*, *375*(6582),
818 eabc4203. https://doi.org/10.1126/science.abc4203
819 Jumper, J., Evans, R., Pritzel, A., Green, T., Figurnov, M., Ronneberger, O., Tunyasuvunakool, K.,
820 Bates, R., Zidek, A., Potapenko, A., Bridgland, A., Meyer, C., Kohl, S. A. A., Ballard, A. J.,
821 Cowie, A., Romera-Paredes, B., Nikolov, S., Jain, R., Adler, J., . . . Hassabis, D. (2021).
822 Highly accurate protein structure prediction with AlphaFold. *Nature*, *596*(7873), 583-
823 589. https://doi.org/10.1038/s41586-021-03819-2
824 Kalatzis, V., Cherqui, S., Antignac, C., & Gasnier, B. (2001). Cystinosin, the protein defective in
825 cystinosis, is a H(+)-driven lysosomal cystine transporter. *EMBO J*, *20*(21), 5940-5949.
826 https://doi.org/10.1093/emboj/20.21.5940
827 Kane, P. M. (1995). Disassembly and reassembly of the yeast vacuolar H(+)-ATPase *in vivo*. *J Biol*
828 *Chem*, *270*(28), 17025-17032. https://www.ncbi.nlm.nih.gov/pubmed/7622524
829 Kang, D. S., Tian, X., & Benovic, J. L. (2014). Role of beta-arrestins and arrestin domain-
830 containing proteins in G protein-coupled receptor trafficking. *Curr Opin Cell Biol*, *27*, 63-
831 71. https://doi.org/10.1016/j.ceb.2013.11.005
832 Kenyon, C., Chang, J., Gensch, E., Rudner, A., & Tabtiang, R. (1993). A *C. elegans* mutant that
833 lives twice as long as wild type. *Nature*, *366*(6454), 461-464.
834 https://doi.org/10.1038/366461a0
835 Khan, A. S., & Frigo, D. E. (2017). A spatiotemporal hypothesis for the regulation, role, and
836 targeting of AMPK in prostate cancer. *Nat Rev Urol*, *14*(3), 164-180.
837 https://doi.org/10.1038/nrurol.2016.272

838 Lapierre, L. R., Gelino, S., Melendez, A., & Hansen, M. (2011). Autophagy and lipid metabolism
839 coordinately modulate life span in germline-less *C. elegans*. *Curr Biol*, *21*(18), 1507-1514.
840 https://doi.org/10.1016/j.cub.2011.07.042
841 Laqtom, N. N., Dong, W., Medoh, U. N., Cangelosi, A. L., Dharamdasani, V., Chan, S. H., Kunchok,
842 T., Lewis, C. A., Heinze, I., Tang, R., Grimm, C., Dang Do, A. N., Porter, F. D., Ori, A.,
843 Sabatini, D. M., & Abu-Remaileh, M. (2022). CLN3 is required for the clearance of
844 glycerophosphodiesters from lysosomes. *Nature*, *609*(7929), 1005-1011.
845 https://doi.org/10.1038/s41586-022-05221-y
846 Lawrence, R. E., & Zoncu, R. (2019). The lysosome as a cellular centre for signalling, metabolism
847 and quality control. *Nat Cell Biol*, *21*(2), 133-142. https://doi.org/10.1038/s41556-018-
848 0244-7
849 Le, S., Josse, J., & Husson, F. (2008). FactoMineR: An R package for multivariate analysis. *Journal*
850 *of statistical software*, *25*(1), 1-18. https://doi.org/10.18637/jss.v025.i01
851 Leger-Silvestre, I., Caffrey, J. M., Dawaliby, R., Alvarez-Arias, D. A., Gas, N., Bertolone, S. J.,
852 Gleizes, P. E., & Ellis, S. R. (2005). Specific Role for Yeast Homologs of the Diamond
853 Blackfan Anemia-associated Rps19 Protein in Ribosome Synthesis. *J Biol Chem*, *280*(46),
854 38177-38185. https://doi.org/10.1074/jbc.M506916200
855 Li, R. J., Xu, J., Fu, C., Zhang, J., Zheng, Y. G., Jia, H., & Liu, J. O. (2016). Regulation of mTORC1 by
856 lysosomal calcium and calmodulin. *Elife*, *5*. https://doi.org/10.7554/eLife.19360
857 Linkert, M., Rueden, C. T., Allan, C., Burel, J. M., Moore, W., Patterson, A., Loranger, B., Moore,
858 J., Neves, C., Macdonald, D., Tarkowska, A., Sticco, C., Hill, E., Rossner, M., Eliceiri, K. W.,

859 & Swedlow, J. R. (2010). Metadata matters: access to image data in the real world. *J Cell*
860 *Biol*, *189*(5), 777-782. https://doi.org/10.1083/jcb.201004104
861 Lubke, T., Lobel, P., & Sleat, D. E. (2009). Proteomics of the lysosome. *Biochim Biophys Acta*,
862 *1793*(4), 625-635. https://doi.org/10.1016/j.bbamcr.2008.09.018
863 Ma, Z., Thomas, K. S., Webb, D. J., Moravec, R., Salicioni, A. M., Mars, W. M., & Gonias, S. L.
864 (2002). Regulation of Rac1 activation by the low density lipoprotein receptor-related
865 protein. *J Cell Biol*, *159*(6), 1061-1070. https://doi.org/10.1083/jcb.200207070
866 Mak, K. H., Zhao, Q., Hu, P.-W., Au-Yeung, C.-L., Yang, J., Duraine, L., Yu, Y., Abu-Remaileh, M.,
867 Sabatini, D., Wang, J. D., & Wang, M. C. (2020). Lysosomal nucleotide metabolism
868 regulates ER proteostasis through mTOR signaling. *bioRxiv*, 2020.2004.2018.048561.
869 https://doi.org/10.1101/2020.04.18.048561
870 Markmann, S., Krambeck, S., Hughes, C. J., Mirzaian, M., Aerts, J. M., Saftig, P., Schweizer, M.,
871 Vissers, J. P., Braulke, T., & Damme, M. (2017). Quantitative Proteome Analysis of
872 Mouse Liver Lysosomes Provides Evidence for Mannose 6-phosphate-independent
873 Targeting Mechanisms of Acid Hydrolases in Mucolipidosis II. *Mol Cell Proteomics*, *16*(3),
874 438-450. https://doi.org/10.1074/mcp.M116.063636
875 Martins, R., Lithgow, G. J., & Link, W. (2016). Long live FOXO: unraveling the role of FOXO
876 proteins in aging and longevity. *Aging Cell*, *15*(2), 196-207.
877 https://doi.org/10.1111/acel.12427
878 Mayer, M. P. (2010). Gymnastics of molecular chaperones. *Mol Cell*, *39*(3), 321-331.
879 https://doi.org/10.1016/j.molcel.2010.07.012

880 McGuire, C. M., & Forgac, M. (2018). Glucose starvation increases V-ATPase assembly and
881 activity in mammalian cells through AMP kinase and phosphatidylinositide 3-kinase/Akt
882 signaling. *J Biol Chem*, *293*(23), 9113-9123. https://doi.org/10.1074/jbc.RA117.001327
883 Mijaljica, D., & Devenish, R. J. (2013). Nucleophagy at a glance. *J Cell Sci*, *126*(Pt 19), 4325-4330.
884 https://doi.org/10.1242/jcs.133090
885 Mutlu, A. S., Gao, S. M., Zhang, H., & Wang, M. C. (2020). Olfactory specificity regulates lipid
886 metabolism through neuroendocrine signaling in *Caenorhabditis elegans*. *Nature*
887 *communications*, *11*(1), 1-15. https://doi.org/10.1038/s41467-020-15296-8
888 Nakae, I., Fujino, T., Kobayashi, T., Sasaki, A., Kikko, Y., Fukuyama, M., Gengyo-Ando, K., Mitani,
889 S., Kontani, K., & Katada, T. (2010). The arf-like GTPase Arl8 mediates delivery of
890 endocytosed macromolecules to lysosomes in *Caenorhabditis elegans*. *Mol Biol Cell*,
891 *21*(14), 2434-2442. https://doi.org/10.1091/mbc.E09-12-1010
892 Nicoli, E. R., Weston, M. R., Hackbarth, M., Becerril, A., Larson, A., Zein, W. M., Baker, P. R., 2nd,
893 Burke, J. D., Dorward, H., Davids, M., Huang, Y., Adams, D. R., Zerfas, P. M., Chen, D.,
894 Markello, T. C., Toro, C., Wood, T., Elliott, G., Vu, M., . . . Malicdan, M. C. V. (2019).
895 Lysosomal Storage and Albinism Due to Effects of a De Novo CLCN7 Variant on
896 Lysosomal Acidification. *Am J Hum Genet*, *104*(6), 1127-1138.
897 https://doi.org/10.1016/j.ajhg.2019.04.008
898 Nishimura, T., Kaizuka, T., Cadwell, K., Sahani, M. H., Saitoh, T., Akira, S., Virgin, H. W., &
899 Mizushima, N. (2013). FIP200 regulates targeting of Atg16L1 to the isolation membrane.
900 *EMBO Rep*, *14*(3), 284-291. https://doi.org/10.1038/embor.2013.6

901 Nixon, R. A., & Cataldo, A. M. (2006). Lysosomal system pathways: genes to neurodegeneration
902 in Alzheimer's disease. *J Alzheimers Dis*, *9*(3 Suppl), 277-289.
903 https://doi.org/10.3233/jad-2006-9s331
904 Pettersen, E. F., Goddard, T. D., Huang, C. C., Couch, G. S., Greenblatt, D. M., Meng, E. C., &
905 Ferrin, T. E. (2004). UCSF Chimera--a visualization system for exploratory research and
906 analysis. *J Comput Chem*, *25*(13), 1605-1612. https://doi.org/10.1002/jcc.20084
907 Platt, F. M., Boland, B., & van der Spoel, A. C. (2012). The cell biology of disease: lysosomal
908 storage disorders: the cellular impact of lysosomal dysfunction. *J Cell Biol*, *199*(5), 723-
909 734. https://doi.org/10.1083/jcb.201208152
910 Popovic, D., & Dikic, I. (2014). TBC1D5 and the AP2 complex regulate ATG9 trafficking and
911 initiation of autophagy. *EMBO Rep*, *15*(4), 392-401.
912 https://doi.org/10.1002/embr.201337995
913 Pu, J., Guardia, C. M., Keren-Kaplan, T., & Bonifacino, J. S. (2016). Mechanisms and functions of
914 lysosome positioning. *J Cell Sci*, *129*(23), 4329-4339. https://doi.org/10.1242/jcs.196287
915 Ramachandran, P. V., Savini, M., Folick, A. K., Hu, K., Masand, R., Graham, B. H., & Wang, M. C.
916 (2019). Lysosomal Signaling Promotes Longevity by Adjusting Mitochondrial Activity. *Dev*
917 *Cell*, *48*(5), 685-696 e685. https://doi.org/10.1016/j.devcel.2018.12.022
918 Ratto, E., Chowdhury, S. R., Siefert, N. S., Schneider, M., Wittmann, M., Helm, D., & Palm, W.
919 (2022). Direct control of lysosomal catabolic activity by mTORC1 through regulation of
920 V-ATPase assembly. *Nat Commun*, *13*(1), 4848. https://doi.org/10.1038/s41467-022-
921 32515-6

922 Rebsamen, M., Pochini, L., Stasyk, T., de Araujo, M. E., Galluccio, M., Kandasamy, R. K., Snijder,
923 B., Fauster, A., Rudashevskaya, E. L., Bruckner, M., Scorzoni, S., Filipek, P. A., Huber, K.
924 V., Bigenzahn, J. W., Heinz, L. X., Kraft, C., Bennett, K. L., Indiveri, C., Huber, L. A., &
925 Superti-Furga, G. (2015). SLC38A9 is a component of the lysosomal amino acid sensing
926 machinery that controls mTORC1. *Nature*, *519*(7544), 477-481.
927 https://doi.org/10.1038/nature14107
928 Saltzman, A. B., Leng, M., Bhatt, B., Singh, P., Chan, D. W., Dobrolecki, L., Chandrasekaran, H.,
929 Choi, J. M., Jain, A., Jung, S. Y., Lewis, M. T., Ellis, M. J., & Malovannaya, A. (2018).
930 gpGrouper: A Peptide Grouping Algorithm for Gene-Centric Inference and Quantitation
931 of Bottom-Up Proteomics Data. *Mol Cell Proteomics*, *17*(11), 2270-2283.
932 https://doi.org/10.1074/mcp.TIR118.000850
933 Savini, M., Folick, A., Lee, Y. T., Jin, F., Cuevas, A., Tillman, M. C., Duffy, J. D., Zhao, Q., Neve, I.
934 A., Hu, P. W., Yu, Y., Zhang, Q., Ye, Y., Mair, W. B., Wang, J., Han, L., Ortlund, E. A., &
935 Wang, M. C. (2022). Lysosome lipid signalling from the periphery to neurons regulates
936 longevity. *Nat Cell Biol*, *24*(6), 906-916. https://doi.org/10.1038/s41556-022-00926-8
937 Savini, M., Zhao, Q., & Wang, M. C. (2019). Lysosomes: Signaling Hubs for Metabolic Sensing
938 and Longevity. *Trends Cell Biol*, *29*(11), 876-887.
939 https://doi.org/10.1016/j.tcb.2019.08.008
940 Schroder, B. A., Wrocklage, C., Hasilik, A., & Saftig, P. (2010). The proteome of lysosomes.
941 *Proteomics*, *10*(22), 4053-4076. https://doi.org/10.1002/pmic.201000196
942 Snyder, J. C., Rochelle, L. K., Lyerly, H. K., Caron, M. G., & Barak, L. S. (2013). Constitutive
943 Internalization of the Leucine-rich G Protein-coupled Receptor-5 (LGR5) to the Trans-

944 Golgi Network. *Journal of Biological Chemistry*, *288*(15), 10286-10297.
945 https://doi.org/10.1074/jbc.M112.447540
946 Stiernagle, T. (2006). Maintenance of *C. elegans*. *WormBook*, 1-11.
947 https://doi.org/10.1895/wormbook.1.101.1
948 Stransky, L. A., & Forgac, M. (2015). Amino Acid Availability Modulates Vacuolar H+-ATPase
949 Assembly. *J Biol Chem*, *290*(45), 27360-27369.
950 https://doi.org/10.1074/jbc.M115.659128
951 Sugiura, T., Iga, T., Asai, T., & Mizokami, K. (1989). [Studies on diameter distribution of axons in
952 the optic pathway in human glaucoma]. *Nippon Ganka Gakkai Zasshi*, *93*(11), 1075-
953 1080. https://www.ncbi.nlm.nih.gov/pubmed/2603855
954 Sun, Y., Li, M., Zhao, D., Li, X., Yang, C., & Wang, X. (2020). Lysosome activity is modulated by
955 multiple longevity pathways and is important for lifespan extension in *C. elegans*. *Elife*,
956 *9*, e55745. https://doi.org/10.7554/eLife.55745
957 Turk, V., Stoka, V., Vasiljeva, O., Renko, M., Sun, T., Turk, B., & Turk, D. (2012). Cysteine
958 cathepsins: from structure, function and regulation to new frontiers. *Biochim Biophys*
959 *Acta*, *1824*(1), 68-88. https://doi.org/10.1016/j.bbapap.2011.10.002
960 Varadi, M., Anyango, S., Deshpande, M., Nair, S., Natassia, C., Yordanova, G., Yuan, D., Stroe, O.,
961 Wood, G., Laydon, A., Zidek, A., Green, T., Tunyasuvunakool, K., Petersen, S., Jumper, J.,
962 Clancy, E., Green, R., Vora, A., Lutfi, M., . . . Velankar, S. (2022). AlphaFold Protein
963 Structure Database: massively expanding the structural coverage of protein-sequence
964 space with high-accuracy models. *Nucleic Acids Res*, *50*(D1), D439-D444.
965 https://doi.org/10.1093/nar/gkab1061

966 Vasu, S., Shah, S., Orjalo, A., Park, M., Fischer, W. H., & Forbes, D. J. (2001). Novel vertebrate
967 nucleoporins Nup133 and Nup160 play a role in mRNA export. *J Cell Biol*, *155*(3), 339-
968 354. https://doi.org/10.1083/jcb.200108007
969 Wang, M. C., O'Rourke, E. J., & Ruvkun, G. (2008). Fat metabolism links germline stem cells and
970 longevity in *C. elegans*. *Science*, *322*(5903), 957-960.
971 https://doi.org/10.1126/science.1162011
972 Wang, S., Tsun, Z. Y., Wolfson, R. L., Shen, K., Wyant, G. A., Plovanich, M. E., Yuan, E. D., Jones,
973 T. D., Chantranupong, L., Comb, W., Wang, T., Bar-Peled, L., Zoncu, R., Straub, C., Kim,
974 C., Park, J., Sabatini, B. L., & Sabatini, D. M. (2015). Metabolism. Lysosomal amino acid
975 transporter SLC38A9 signals arginine sufficiency to mTORC1. *Science*, *347*(6218), 188-
976 194. https://doi.org/10.1126/science.1257132
977 Webb, B. A., Aloisio, F. M., Charafeddine, R. A., Cook, J., Wittmann, T., & Barber, D. L. (2021).
978 pHLARE: a new biosensor reveals decreased lysosome pH in cancer cells. *Mol Biol Cell*,
979 *32*(2), 131-142. https://doi.org/10.1091/mbc.E20-06-0383
980 Willett, R., Martina, J. A., Zewe, J. P., Wills, R., Hammond, G. R. V., & Puertollano, R. (2017).
981 TFEB regulates lysosomal positioning by modulating TMEM55B expression and JIP4
982 recruitment to lysosomes. *Nat Commun*, *8*(1), 1580. https://doi.org/10.1038/s41467-
983 017-01871-z
984 Wyant, G. A., Abu-Remaileh, M., Wolfson, R. L., Chen, W. W., Freinkman, E., Danai, L. V., Vander
985 Heiden, M. G., & Sabatini, D. M. (2017). mTORC1 Activator SLC38A9 Is Required to Efflux
986 Essential Amino Acids from Lysosomes and Use Protein as a Nutrient. *Cell*, *171*(3), 642-
987 654 e612. https://doi.org/10.1016/j.cell.2017.09.046

988 Zhang, C. S., Jiang, B., Li, M., Zhu, M., Peng, Y., Zhang, Y. L., Wu, Y. Q., Li, T. Y., Liang, Y., Lu, Z.,
989 Lian, G., Liu, Q., Guo, H., Yin, Z., Ye, Z., Han, J., Wu, J. W., Yin, H., Lin, S. Y., & Lin, S. C.
990 (2014). The lysosomal v-ATPase-Ragulator complex is a common activator for AMPK and
991 mTORC1, acting as a switch between catabolism and anabolism. *Cell Metab*, *20*(3), 526-
992 540. https://doi.org/10.1016/j.cmet.2014.06.014

993

994 **FIGURES AND FIGURE LEGENDS**

995

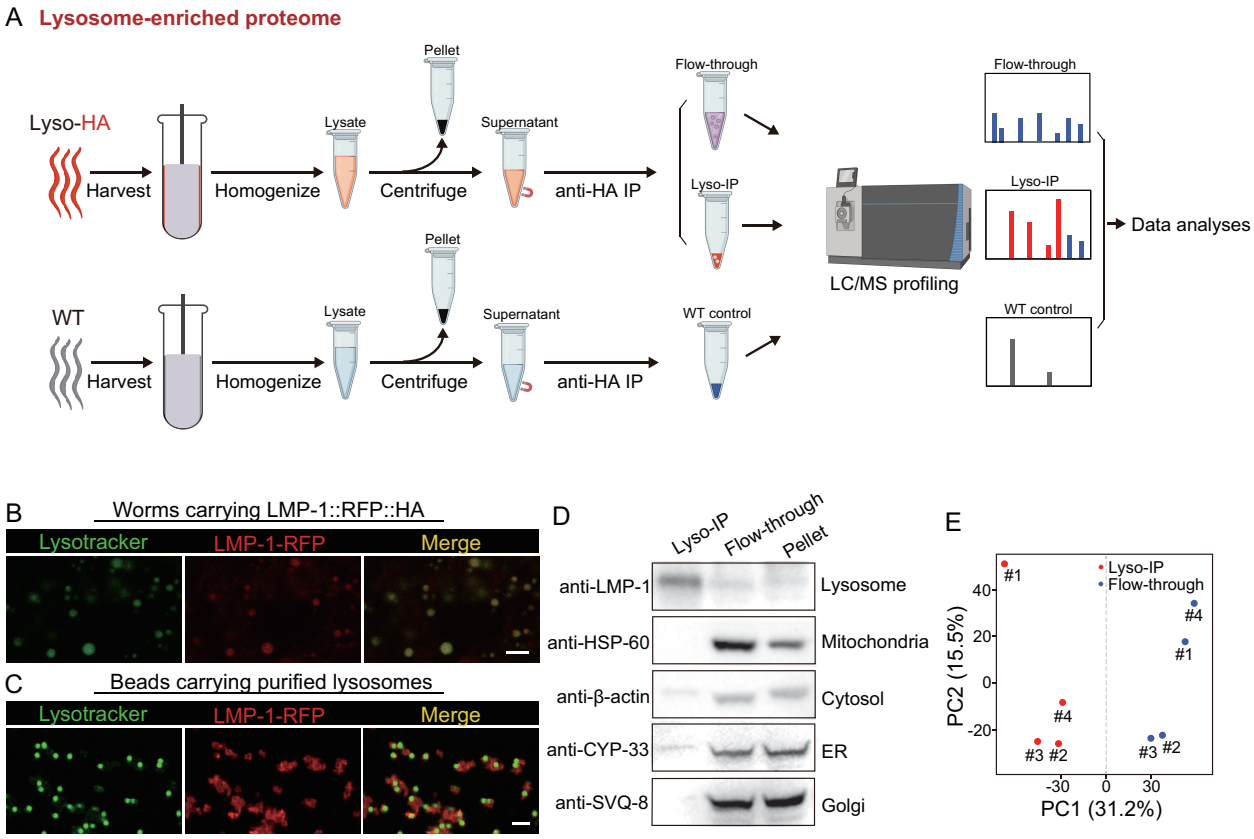

996

997 **Figure 1. Rapid lysosome isolation coupled with proteomic profiling**

998 (**A)** Schematic of the workflow for immunoprecipitation-based lysosome purification (Lyso-IP)
999 and mass-spectrometry based proteomic profiling to identify lysosome-enriched proteomes in *C.*
1000 *elegans.*
1001 (**B**) Example images of transgenic strains carrying LMP-1 Lyso-Tag (LMP-1::RFP-3×HA) with
1002 LysoTracker staining to mark lysosomes *in vivo*. Scale bar=5 μm.
1003 (**C**) Example images of beads carrying purified lysosomes from Lyso-IP with LysoTracker
1004 staining to mark intact lysosomes *in vitro.* Scale bar=5 μm.
1005 (**D**) Western blot for protein markers of different subcellular compartments using purified
1006 lysosomes (Lyso-IP), paired non-lysosomal fractions (Flow-through) or Pellet.
1007 (**E**) PCA analysis of four independent biological replicates of Lyso-IP and Flow-through
1008 samples.
1009

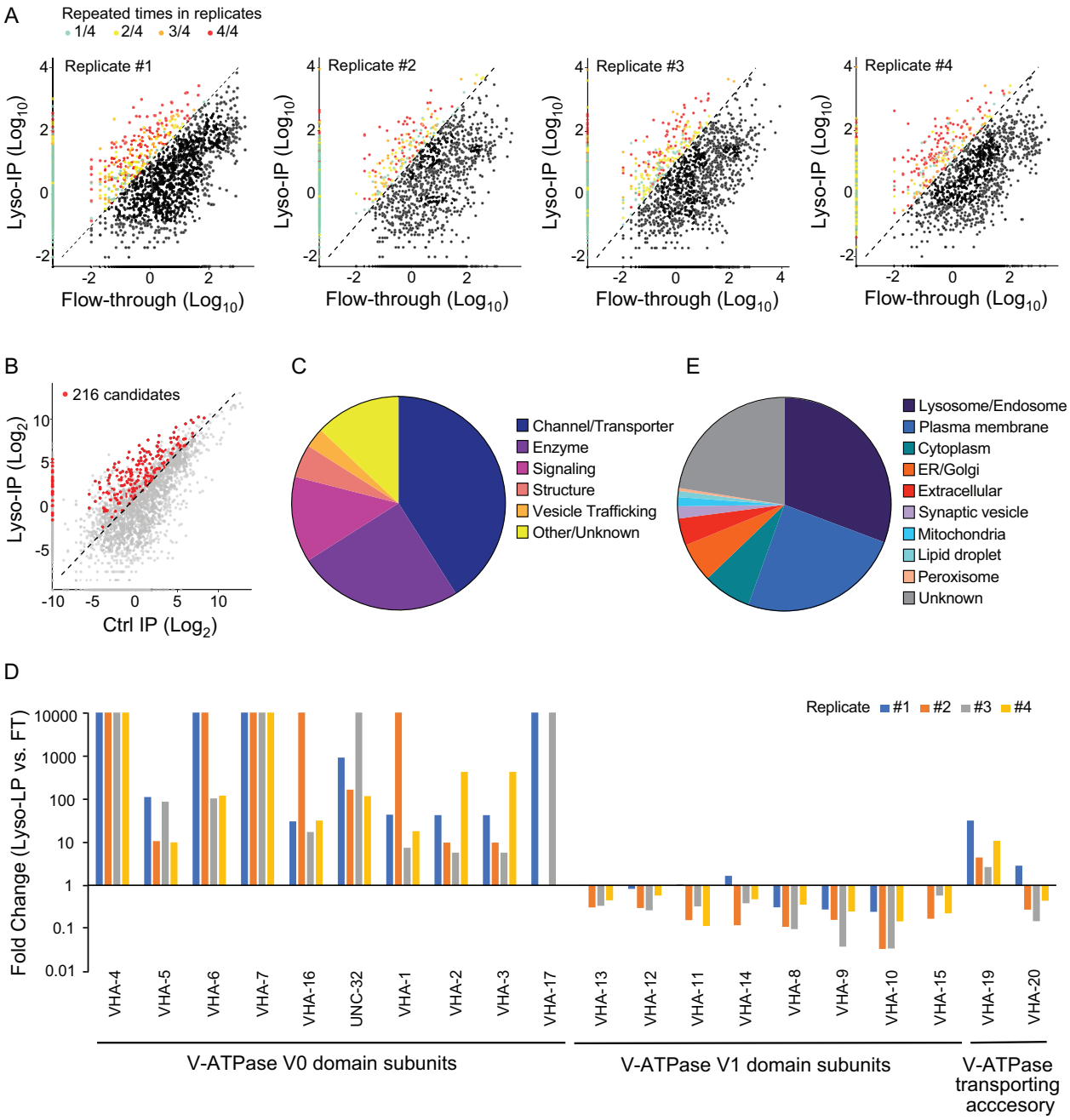

1010

1011 **Figure 2. Systemic view of lysosome-enriched proteome**

1012 (**A**) Scatter plots showing candidate selection from four independent biological replicates in

1013 proteomics analyses. Proteins with at least 10-fold higher levels in Lyso-IP samples than in flow-

1014 through controls are highlighted with different colors based on repeated times in four replicates.

1015 (**B**) Scatter plot showing candidate selection with normalization to non-tagged controls using
1016 wild-type worms. 216 proteins with over 2-fold higher levels in Lyso-IP samples than in non-
1017 tagged controls are highlighted in red.
1018 (**C**) Pie chart showing molecular function categories of lysosome-enriched proteins.
1019 (**D**) The lysosomal enrichment ratio (Lyso-IP vs FT) for each subunit of lysosomal vacuolar
1020 ATPase (v-ATPase) in four independent replicates is shown.
1021 (**E)** Pie chart showing subcellular location categories of lysosome-enriched proteins.
1022

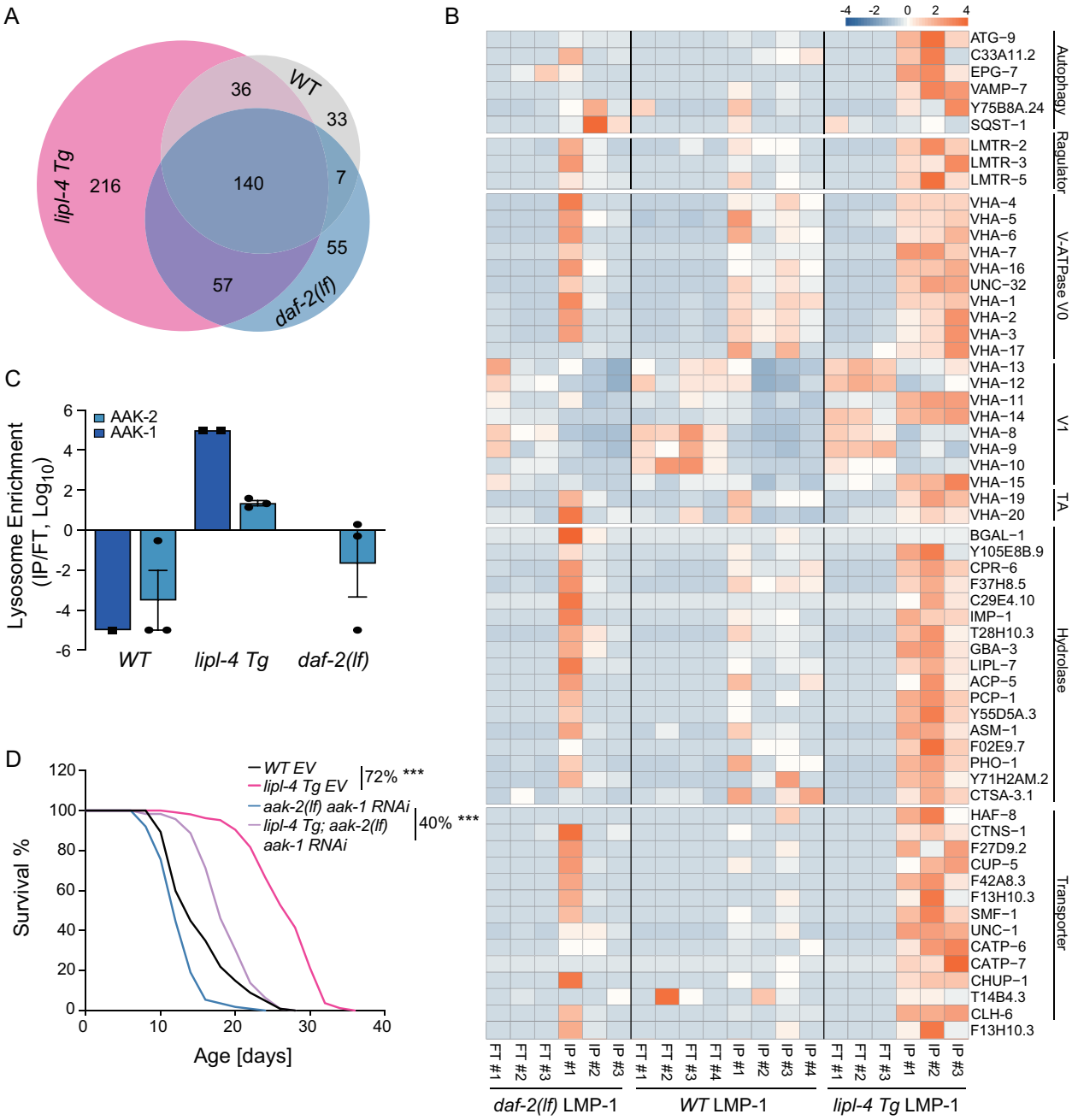

1023

1024 **Figure 3. Lysosome-enriched proteome associated with longevity**

1025 (**A**) Venn diagram showing overlaps among lysosome-enriched proteomes from wild-type (WT),

1026 *lipl-4 Tg* and *daf-2(lf)* worms.

1027 (**B**) Normalized protein levels (z-score across samples) of autophagy-related components,

1028 mTORC1 signaling factors, lysosomal v-ATPase V0, V1 and transporting accessory (TA)

1029 subunits, lysosomal hydrolases and transporter proteins from LMP-1 Lyso-IP proteomic analyses

1030 of WT, *lipl-4 Tg* and *daf-2(lf)*) worms.

1031 (**C**) The lysosomal enrichment ratio (Lyso-IP vs FT) for two homologs of AMPK catalytic

1032 subunits, AAK-1 and AAK-2 in WT, *lipl-4 Tg* and *daf-2(lf)*) worms.

1033 (**D**) Reduction of AMPK using the loss-of-function mutant of *aak-2, aak-2(lf)* together with *aak-*

1034 *1* RNAi knockdown reduces the lifespan extension in the *lipl-4 Tg* worms from 72% to 40%. ***

1035 $p<0.01$ by Log-rank test.

1036

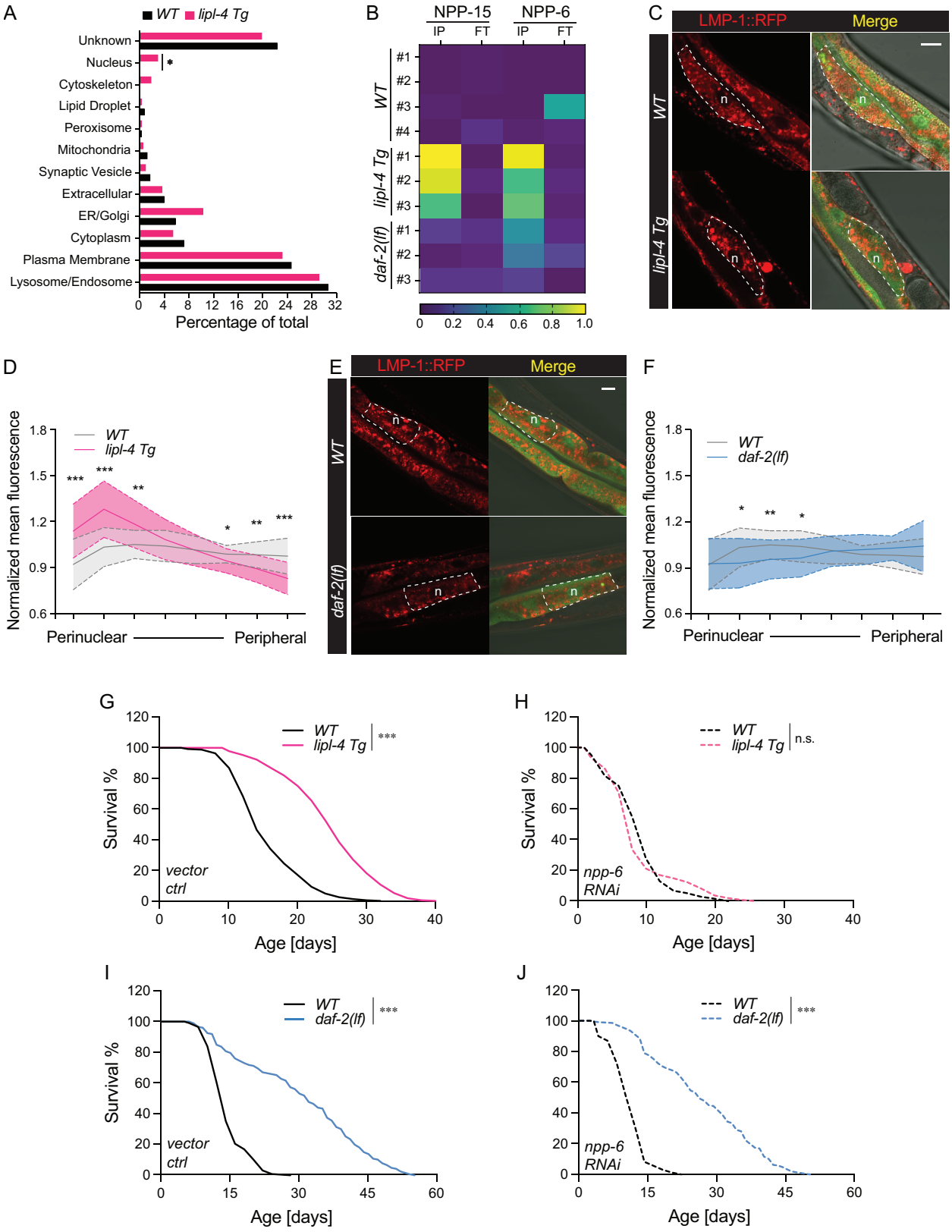

1037

1038 **Figure 4. Enhanced lysosome-nucleus interaction mediating longevity**

1039 **(A)** The percentage of proteins with different subcellular localization is compared between
1040 lysosome-enriched proteomes from WT and *lipl-4 Tg* worms. * $p<0.05$ by 2-sample test for
1041 equality of proportions.
1042 **(B)** Heatmap showing the average levels of nucleoporin proteins NPP-6 and NPP-15 in Lyso-IP
1043 (IP) and flow-through (FT) samples from WT, *lipl-4 Tg* and *daf-2(lf)* worms.
1044 **(C, E)** Representative images of intestinal cells in WT, *lipl-4 Tg* (**C**) and *daf-2(lf)* (**E**) worms
1045 carrying LMP-1::RFP-3×HA and nucleus-enriched GFP, showing the accumulation of
1046 lysosomes around the perinuclear region in the *lipl-4 Tg* but not *daf-2(lf)* worms. Dashed lines
1047 circle intestinal cells and n marks the nucleus. Scale bar=20 μm.
1048 **(D, F)** Line graph showing the spatial distribution of lysosomes from the nuclear to peripheral
1049 region quantified by normalized regional RFP fluorescence signals in intestinal cells of WT, *lipl-*
1050 *4 Tg* (**D**) and *daf-2(lf)* (**F**) worms. N =50 WT /33 *lipl-4 Tg*, 33 WT/ 28 *daf-2(lf)*. Data are
1051 represented as mean ± SD.
1052 **(G-H)** *lipl-4 Tg* worms show lifespan extension compared to WT worms (**G**), which is fully
1053 suppressed by RNAi knockdown of *npp-6* (**H**). ***$p<0.001$, n.s. $p>0.05$ by Log-rank test.
1054 **(I-J)** *daf-2(lf)* worms show lifespan extension compared to WT worms (**I**), which is not affected
1055 by *npp-6* RNAi knockdown (**J**). ***$p<0.001$ by Log-rank test.
1056

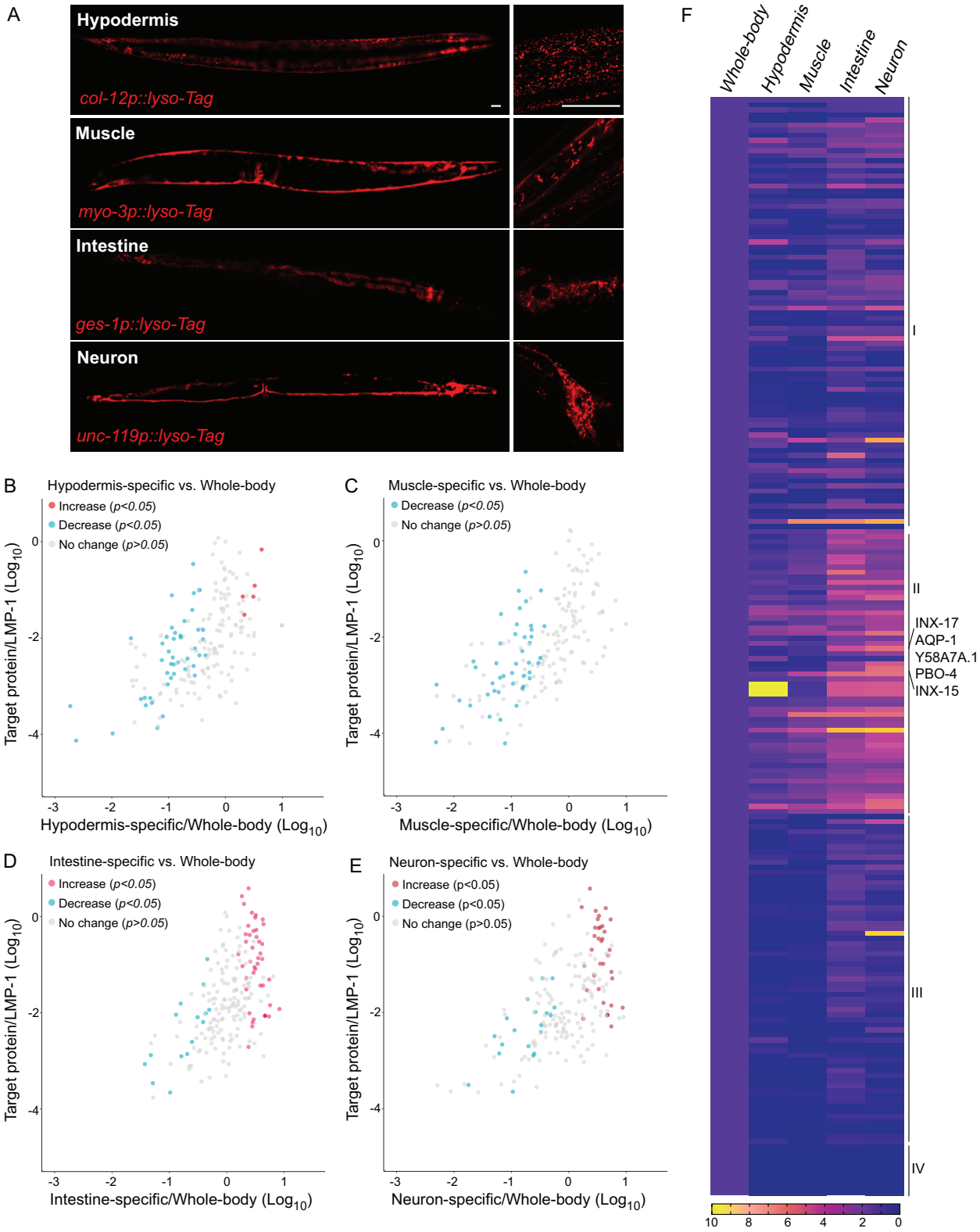

Figure 5. Lysosomal proteome heterogeneity across tissues

1059 **(A)** Example images of transgenic strains carrying Lyso-Tag (LMP-1::RFP-3×HA) driven by
1060 tissue-specific promoters. Scale bar=20 μm.
1061 **(B-E)** Scatter plot showing the relative enrichment ratio for each of 216 lysosome-enriched
1062 proteins identified from whole-body LMP-1 Lyso-IP in comparison with tissue-specific LMP-1
1063 Lyso-IPs, hypodermis (**B**), muscle (**C**), intestine (**D**) and neuron (**E**). X axis, enrichment ratio
1064 tissue-specific vs. whole-body; Y axis, normalized protein abundance over LMP-1; each dot
1065 represents the average of three replicates.
1066 **(F)** Heatmap showing the relative enrichment of 216 lysosome-enriched proteins identified from
1067 whole-body LMP-1 Lyso-IP in comparison with tissue-specific LMP-1 Lyso-IPs. Group I,
1068 comparable ratios between whole-body and tissue-specific Lyso-IPs; Group II, increase in tissue-
1069 specific Lyso-IPs ($p<0.05$ by student's t-test); Group III, decrease in tissue-specific Lyso-IPs
1070 ($p<0.05$ by student's t-test); Group IV, absent in tissue-specific IPs.
1071

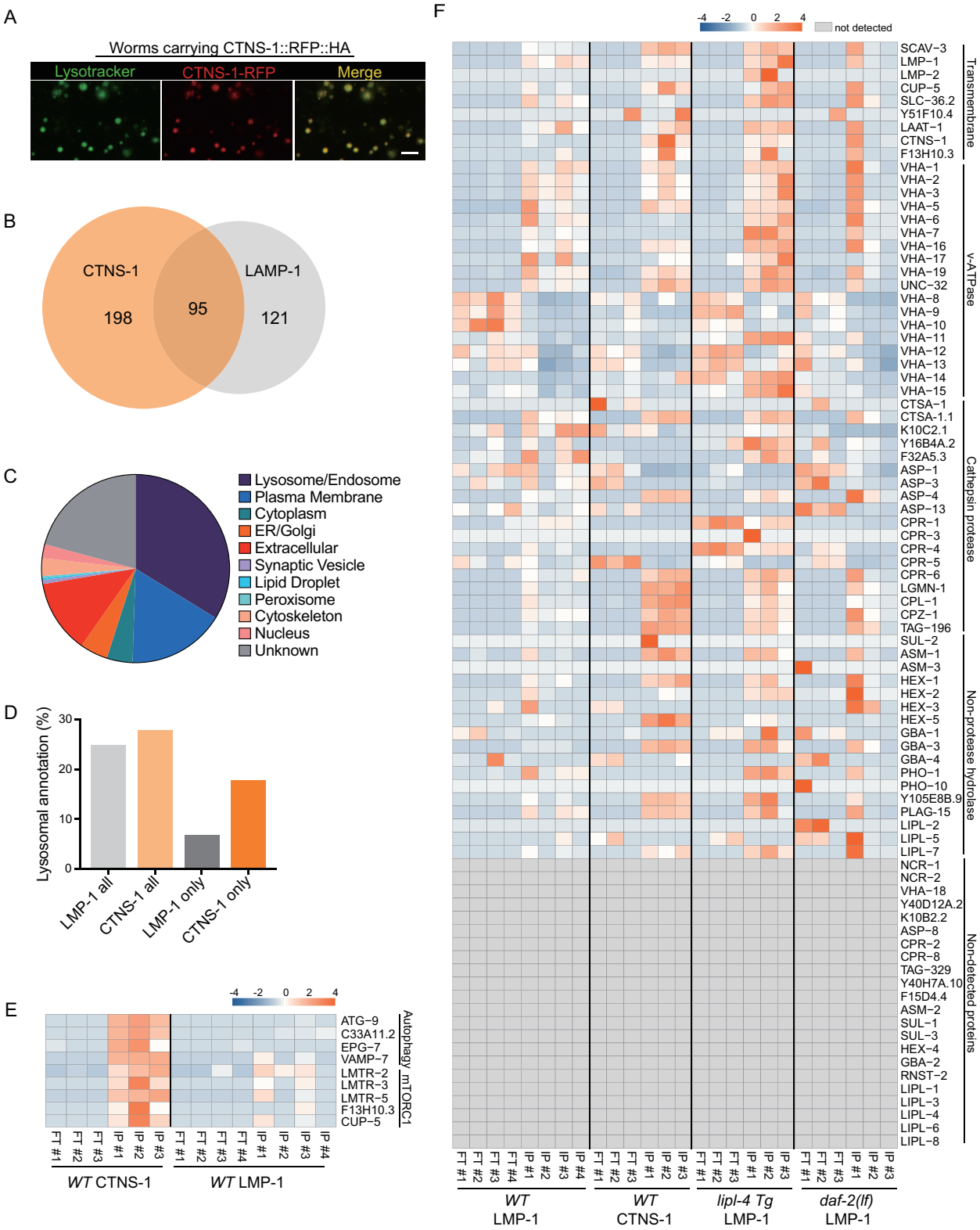

Figure 6. Lysosome-enriched proteome identified with Cystinosin

1074 **(A)** Example images of transgenic strains carrying CTNS-1 Lyso-Tag (CTNS-1::RFP-3×HA)
1075 with LysoTracker staining to mark lysosomes *in vivo*. Scale bar=5 μm.
1076 **(B)** Venn diagram showing the overlap between lysosome-enriched proteomes using LMP-1
1077 Lyso-IP and CTNS-1 Lyso-IP.
1078 **(C)** Pie chart showing subcellular location categories of lysosome-enriched proteins.
1079 **(D)** The proportion of candidates with lysosomal localization annotation in different candidate
1080 groups. "LMP-1 all" and "CTNS-1 all", all candidates from LMP-1 Lyso-IP and CTNS-1 Lyso-
1081 IP, respectively; "LMP-1 only" and "CTNS-1 only", candidates only identified from LMP-1
1082 Lyso-IP or CTNS-1 Lyso-IP, respectively.
1083 **(E)** Normalized protein levels (z-score across samples) of autophagy-related components and
1084 mTORC1 signaling factors from LMP-1 and CTNS-1 Lyso-IP proteomic analyses of WT
1085 worms.
1086 **(F)** Normalized protein levels (z-score across samples) of previously annotated lysosomal
1087 proteins from LMP-1 Lyso-IP proteomic analyses of WT, *lipl-4 Tg* and *daf-2(lf)*) worms and
1088 CTNS-1 Lyso-IP proteomic analyses of WT worms. Proteins not detected by proteomic profiling
1089 are marked in grey.
1090

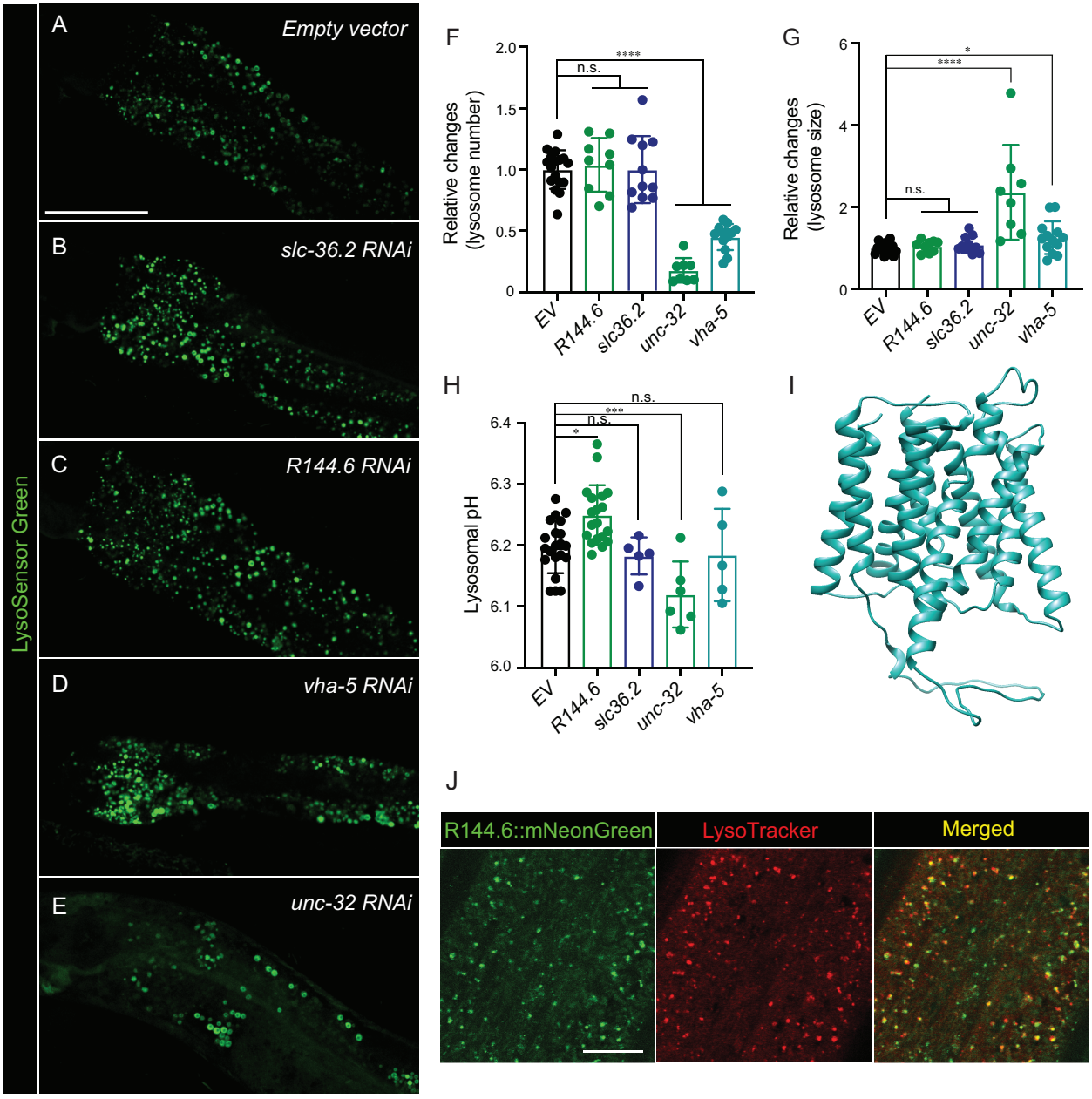

Figure 7. Lysosome-enriched proteins regulating lysosomal functions

(**A-E)** Confocal fluorescence microscopy images of intestinal cells in worms stained with LysoSensor DND-189 and treated with *empty vector* (**A**), *slc36.2* RNAi (**B**), *R144.6* RNAi (**C**), *vha-5* RNAi (**D**) and *unc-32* RNAi (**E**). Scale bar=50 µm.

1096 **(F, G)** RNAi knockdown of *unc-32* or *vha-5* decreases the lysosome number (**F**) but increases
1097 the lysosome size (**G**). The average lysosome number and size per pair of intestinal cells were
1098 quantified. n = 17 (*EV*), 9 (*R144.6*), 11 (*slc36.2*), 8 (*unc-32*), 13 (*vha-5*).
1099 (**H**) RNAi knockdown of *R144.6* and *unc-32* increase and decrease lysosomal pH, respectively.
1100 Lysosomal pH was calculated based on LysoSensor's lifetime measured by Fluorescence
1101 Lifetime Microscopy. n = 21 (*EV*), 19 (*R144.6*), 5 (*slc36.2*), 6 (*unc-32*), 5 (*vha-5*).
1102 **(I)** The structure of the R144.6 protein predicted by AlphaFold2 supports it as a solute carrier
1103 family transporter.
1104 **(J)** Confocal fluorescence microscopy images show that mNeonGreen signals from
1105 endogenously tagged R144.6 colocalize with LysoTracker Red signals in the hypodermis. Scale
1106 bar=10 μm.
1107 (**F**-**H**) Data shown as mean ± SD, *$p<0.05$; **$p<0.01$, ***$p<0.001$, ****$p<0.0001$, n.s. $p>0.05$
1108 by Student's t-test (unpaired, two-tailed).
1109

1110 **SUPPLEMENTARY FIGURES**

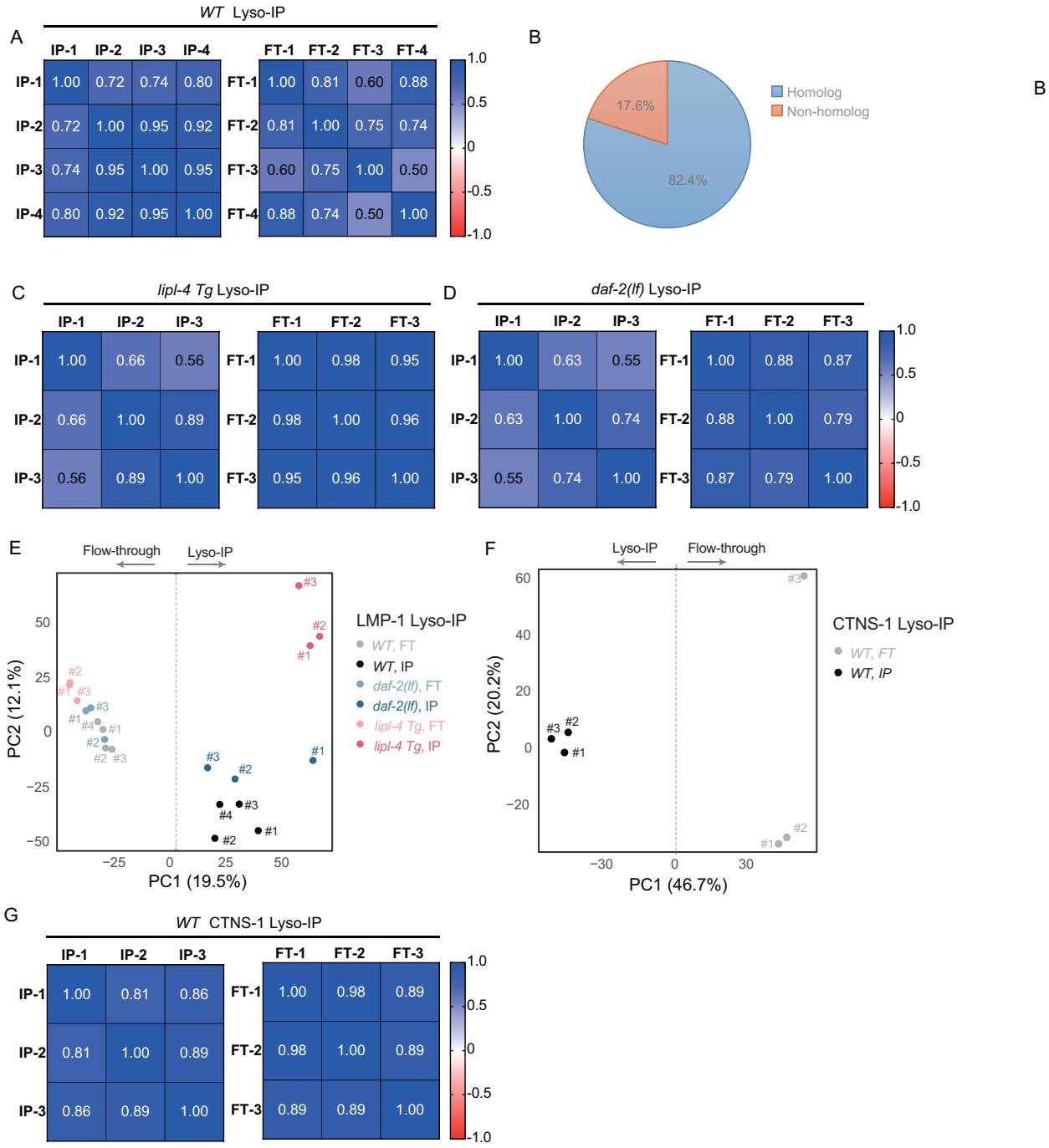

1111

1112 **Supplementary Figure 1. Lyso-IP analyses from worms with different genotypes**

1113 (**A**) Correlation analysis of four independent biological replicates of Lyso-IP (IP) and Flow-

1114 through (FT) samples from proteomics analyses.

1115 **(B)** Pie chart showing the proportion of LMP-1 Lyso-IP candidates from WT worms with
1116 mammalian homologs.
1117 (**C** and **D)** Correlation analysis of three independent biological replicates of Lyso-IP (IP) and
1118 Flow-through (FT) from proteomics analyses of the long-lived *lipl-4* transgenic strain (*lipl-4 Tg*,
1119 **C**) and the *daf-2* loss-of-function mutant (*daf-2(lf)*), **D**).
1120 **(E)** PCA analysis of Lyso-IP replicates and flow-through controls in LMP-1 Lyso-IP of WT,
1121 *lipl-4 Tg* and *daf-2(lf)* worms.
1122 **(F)** PCA analysis of Lyso-IP replicates and flow-through controls of CTNS-1 Lyso-IP of WT
1123 worms.
1124 **(G)** Correlation analysis of three independent biological replicates of Lyso-IP (IP) and Flow-
1125 through (FT) samples from proteomic analyses of CTNS-1 Lyso-IP.
1126

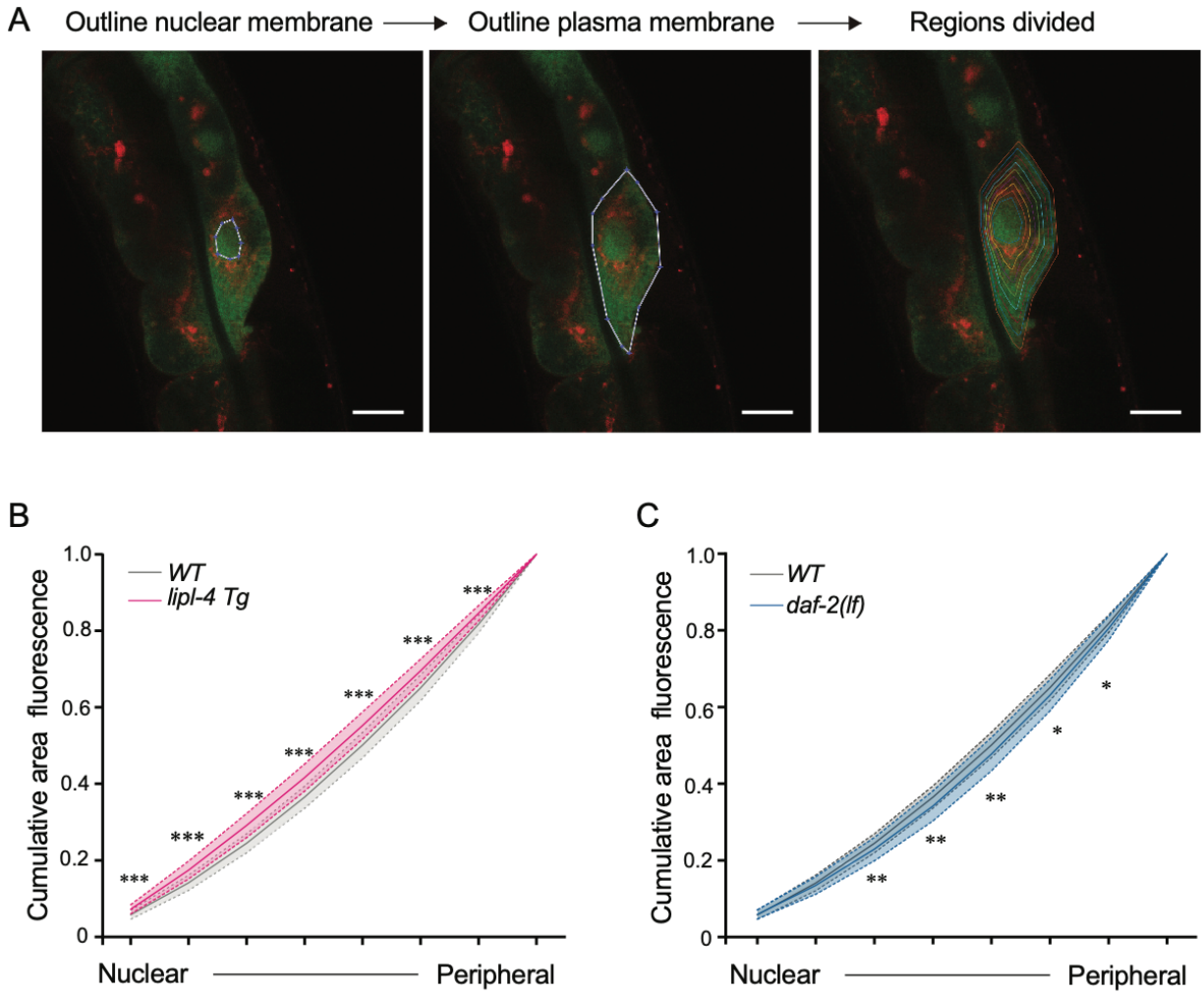

Supplementary Figure 2. Quantitative analysis of lysosomal positioning

(**A**) Brief summary of the method flow for quantifying the lysosomal distribution in intestinal cells of *C. elegans*. Scale bar=10 µm.

(B, C) Curve graph showing the normalized accumulated intensity of lysosomal signals from the nuclear to the peripheral region in WT, *lipl-4 Tg* (**B**) and *daf-2(lf)* (**C**) animals. *$p<0.05$; **$p<0.01$, ***$p<0.001$, ****$p<0.0001$, n.s. $p>0.05$ by Student's t-test (unpaired, two-tailed) for each region. N =50 WT /33 *lipl-4 Tg*, 33 WT/ 28 *daf-2(lf)*. Data are represented as mean ± SD.

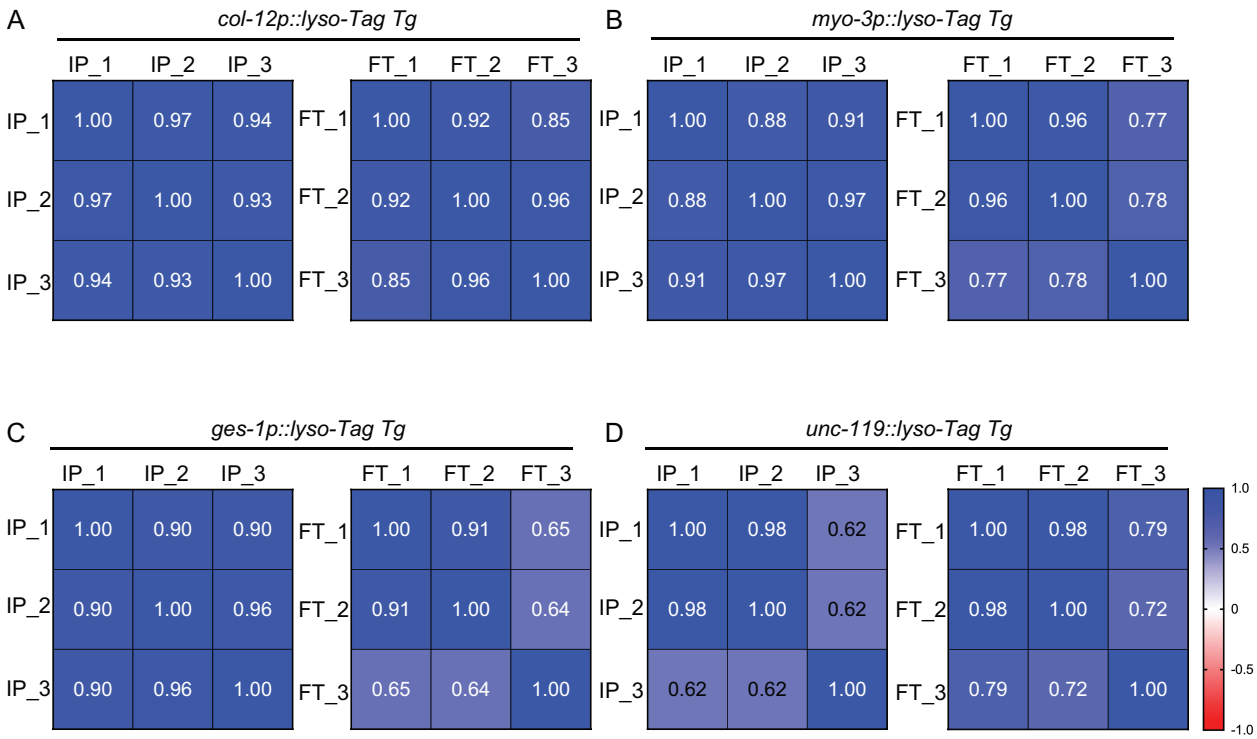

Supplementary Figure 3. Correlation analyses of tissue-specific Lyso-IPs

(A-D) Pearson Correlation matrices of tissue-specific lyso-IP (IP) samples and flow-through (FT) samples show the correlation among three different replicates. **(A)** Hypodermis, **(B)** Muscle, **(C)** Intestine, **(D)** Neuron.

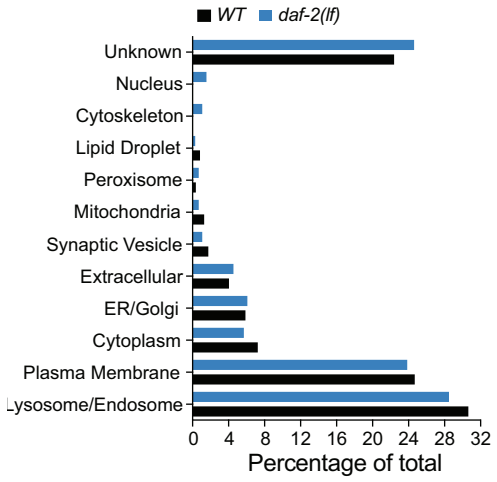

Supplementary Figure 4. Subcellular category analyses of *daf-2(lf)* candidates

1144 The percentage of proteins with different subcellular localization is compared between

1145 lysosome-enriched proteomes from WT and *daf-2(lf)* worms.

1146

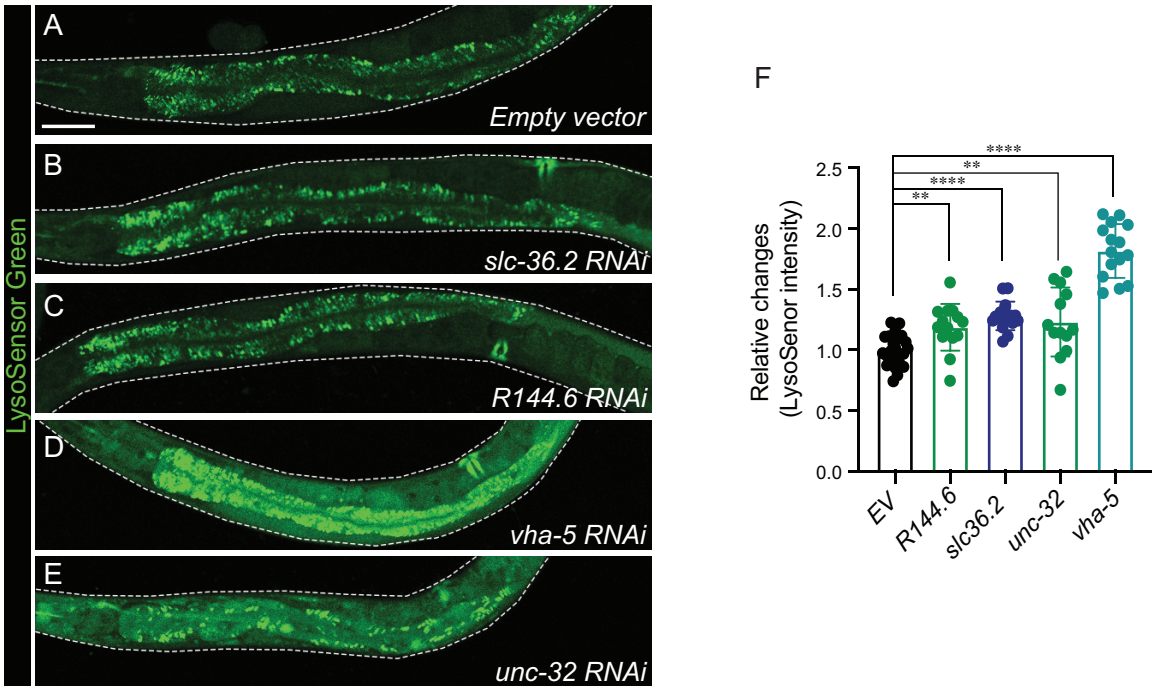

1147

1148 **Supplementary Figure 5. Inactivation of lysosome-enriched candidates increases**

1149 **LysoSensor signal intensity**

1150 (**A-E)** Confocal fluorescence microscopy images of intestinal cells in worms stained with

1151 LysoSensor DND-189 and treated with *empty vector* (**A**), *slc36.2* RNAi (**B**), *R144.6* RNAi (**C**),

1152 *vha-5* RNAi (**D**) and *unc-32* RNAi (**E**). Scale bar=50 µm.

1153 **(F)** RNAi knockdown of *slc36.2, R144.6, unc-32 or vha-5* increases the LysoSensor signal

1154 intensity in the area of the first pair of intestinal cells. n = 24 (*EV*), 14 (*R144.6*), 13 (*slc36.2*), 15

1155 (*unc-32*), 16 (*vha-5*). *$p<0.05$; **$p<0.01$, ***$p<0.001$, ****$p<0.0001$, n.s. $p>0.05$ by Student's

1156 t-test (unpaired, two-tailed).

1157

1158 **Supplementary Table 1. Lysosome-enriched proteins identified from LMP-1 Lyso-IP using**

1159 **WT worms**

1160 **Supplementary Table 2. Lysosome-enriched proteins identified from LMP-1 Lyso-IP using**

1161 ***lipl-4 Tg* worms**

1162 **Supplementary Table 3. Summary of lifespan analyses**

1163 **Supplementary Table 4. Lysosome-enriched proteins identified from LMP-1 Lyso-IP using**

1164 ***daf-2(lf)* mutant**

1165 **Supplementary Table 5. Lysosome-enriched proteome exhibits tissue-specificity**

1166 **Supplementary Table 6. Lysosome-enriched proteins identified from CTNS-1 Lyso-IP**

1167 **using WT worms**

1168 **Supplementary Table 7. LysoSensor screening of lysosome-enriched proteins shared**

1169 **between LMP-1 and the CTNS-1 Lyso-Ips**

1170 **Supplementary code. Matlab codes for lysosome distribution quantification**